

Synoptic-Scale Waves in Sheared Background Flow over the Western North Pacific

TAO FENG AND XIU-QUN YANG

China Meteorological Administration–Nanjing University Joint Laboratory for Climate Prediction Studies, Institute for Climate and Global Change Research, School of Atmospheric Sciences, Nanjing University, Nanjing, China

WEN ZHOU

Guy Carpenter Asia-Pacific Climate Impact Center, School of Energy and Environment, City University of Hong Kong, Hong Kong, China

RONGHUI HUANG AND LIANG WU

Center for Monsoon System Research, Institute of Atmospheric Physics, Chinese Academy of Sciences, Beijing, China

DEJIAN YANG

China Meteorological Administration–Nanjing University Joint Laboratory for Climate Prediction Studies, Institute for Climate and Global Change Research, School of Atmospheric Sciences, Nanjing University, Nanjing, China

(Manuscript received 25 February 2016, in final form 6 August 2016)

ABSTRACT

Tropical depression (TD)-type waves are the dominant mode of synoptic-scale fluctuations over the western North Pacific. By applying spatiotemporal filters to the observed OLR data and the NCEP–DOE AMIP-II reanalysis data for 1979–2013, this study reveals the characteristics and energetics of convectively coupled TD-type waves under the effects of different circulation patterns in association with vertical wind shear. Results exhibit that different ambient sheared flows significantly affect the vertical structure of westward-propagating TD-type waves, with a lower-tropospheric mode in an easterly sheared background and an upper-tropospheric mode in a westerly sheared background. Energetic diagnoses demonstrate that when the disturbance is trapped in the lower (upper) level by easterly (westerly) shear, the horizontal mean flow in the lower (upper) level favors wave growth by converting energy from the shear of the zonal mean flow (from the convergence of the meridional mean flow). During the penetration of a westward-propagating synoptic-scale disturbance from a westerly sheared flow into an easterly sheared flow, the upper-level disturbance decays, and the lower-level disturbance intensifies. Meanwhile, the upper-level kinetic energy is transferred downward, but the effect induces the wave growth only confined to the midlevels. Consequently, the low-level growth of the westward-propagating upper-level synoptic-scale disturbance is mainly attributed to the barotropic conversion of horizontal mean flow in the lower troposphere.

1. Introduction

Tropical depression (TD)-type waves, which are sometimes called easterly waves, are the dominant mode of the synoptic-scale perturbations that prevail over the western North Pacific during the boreal summer. The initiation of

TD-type waves may be attributed to instability of the summertime mean flow (Li 2006), extratropical forcing in the upper troposphere with southward and downward wave activity (Tam and Li 2006), Rossby energy dispersion from a mature tropical cyclone (Ge et al. 2008; Krouse et al. 2008; Chen and Tam 2012), or the transition from equatorial mixed Rossby–gravity (MRG) waves (Takayabu and Nitta 1993; Dickinson and Molinari 2002; Aiyyer and Molinari 2003). These TD-type waves significantly affect the weather and climate: for example, precipitation (Schreck et al. 2011, 2012), convection

Corresponding author address: Prof. Xiu-Qun Yang, School of Atmospheric Sciences, Nanjing University, 163 Xianlin Avenue, Nanjing 210023, China.
E-mail: xqyang@nju.edu.cn

activity (Xu et al. 2014; Park et al. 2015), and tropical cyclones (Frank and Roundy 2006; Fu et al. 2007; Chen and Chou 2014) over the western North Pacific and the East Asian seacoast.

The three-dimensional structure of typical TD-type waves over the western North Pacific has been known for decades. Previous observational studies have identified these synoptic-scale waves based on their typical horizontal characteristics: that is, northwest–southeast-oriented wave trains with alternating cyclonic and anticyclonic disturbances, with a wavelength of approximately 2500 km and a period of 3–8 days (Reed and Recker 1971; Wallace 1971; Lau and Lau 1990; Takayabu and Nitta 1993). One important feature of these TD-type waves is the coincidence between deep convection and vortex circulation (Takayabu and Nitta 1993; Dickinson and Molinari 2002). This feature implies that circulation and convective diabatic heating are strongly coupled. These waves propagate northwestward over the western North Pacific, and the direction and speed are sensitive to the summertime mean flow. Numerical studies suggest that these synoptic-scale waves move more poleward during El Niño years (Chen 2012). Additionally, westward-propagating tropical waves can be decelerated through a Doppler shift effect (Han and Khouider 2010; Wu et al. 2015a). Furthermore, there is also a horizontal deformation effect on the equatorial waves by the basic state. Webster and Chang (1988) proposed that the zonally convergent basic flow could contract the horizontal scale of transient eddies in the wave accumulation zone. In the presence of a meridionally sheared zonal flow, the wave structure becomes meridionally asymmetric, and its axis tilts eastward with increasing latitude (Nitta and Yanai 1969; Lipps 1970; Xie and Wang 1996; Wu et al. 2015b). The eastward tilt of the wave axis is also an indicator of energy transition from basic flow to eddies through barotropic instability.

Vertically, the maximum wind perturbations near the upper and lower troposphere exhibit a TD-type disturbance, and a remarkable warm core forms a warm-temperature anomaly at intermediate levels and cold anomalies above and below the core (Reed and Recker 1971; Nitta and Takayabu 1985; Lau and Lau 1990). By using sounding data over the tropical western North Pacific, Reed and Recker (1971) examined the composite structure and properties of 18 TD-type disturbances. Interestingly, they found that the vertical structure of a TD-type disturbance systematically evolves with longitude such that the wave axis tilts eastward with height near the central Pacific and gradually tilts westward while traversing westward. They attributed this to the zonal change in the basic vertical wind shear. Additionally, they found that the relative position between

low-level disturbances and coupled convective precipitation also changes in a systematic fashion across the western Pacific. These features are generally consistent with the modeling and theoretical study by Holton (1971). The systematic variation in the vertical structure of the TD-type disturbances with longitude has also been observed in other studies. Wallace (1971) found that the low-level convergence maximum of a disturbance rises to higher levels as the waves propagate westward. Tam and Li (2006) revealed that the perturbation maxima of tropical summertime TD-type waves occurred near 200 hPa east of 150°E but occurred in the middle and lower troposphere west of 150°E. Serra et al. (2008) examined the horizontal and vertical structure of TD-type waves in the eastern-central Pacific, and they also found systematic variations in these waves similar to the findings of Reed and Recker (1971). However, most of these studies examined the vertical structures of TD-type waves at different longitudes, whereas few studies have focused on the wave structures under different sheared environments over the western North Pacific, which could provide better understanding of the role of vertically sheared ambient flow in regulating the synoptic-scale waves.

As mentioned above, the structure of TD-type waves is affected by the vertical shear of the zonal mean flow. Webster and Chang (1998) suggested the importance of easterly wind shear in trapping Rossby wave energy in the lower troposphere and noted that easterly shear inhibits vertical propagation while westerly shear enhances it. From numerical experiments, Li (2006) demonstrated that an easterly (westerly) shear may result in faster (slower) growth of eddies in the lower troposphere and a more poleward (equatorward) shift. How does vertical wind shear affect waves in different levels? Using a two-layer equatorial β -plane model, Wang and Xie (1996) proposed a coupling effect of vertical wind shear, in which constant vertical wind shear modulates the phase difference between the barotropic and baroclinic components of a Rossby wave, thereby trapping the perturbation in the lower (upper) troposphere in easterly (westerly) sheared environments. Furthermore, Xie and Wang (1996) suggested that moderate wind shear destroys wave stability by generating stronger Ekman pumping-induced heating and meridional heat flux, which feeds the mean available potential energy to eddies. In addition, Molinari et al. (2007) indicated that easterly vertical shear would trap an equatorial Rossby (ER) wave packet in the lower troposphere because of the coupling effect. Yang et al. (2003) proposed that nonzero ambient flow has a Doppler shift effect on westward-propagating MRG waves, and whether the wave propagates in the upper or lower troposphere

could be explained by the Doppler shift of the mean flow. Moreover, they suggested that the lower-level (upper-level) MRG waves are more likely to be found in the western hemisphere (eastern hemisphere), where westerly (easterly) shear prevails as a result of the Doppler shift effect. Nevertheless, [Ge et al. \(2007\)](#) noted that the coupling effect of the vertical wind shear plays a more dominant role than Doppler shift in regulating wave structure after a preliminary numerical study on the role of vertical wind shear on the synoptic-scale Rossby waves, which are excited by a mature tropical cyclone.

Vertical wind shear varies with longitude during the summer over the western North Pacific so that easterly shear appears in the west and westerly shear appears in the east. Consequently, when tropical disturbances propagate westward from the eastern Pacific, they usually encounter easterly sheared ambient flow. Therefore, upper-level disturbances are weakened, and lower-level disturbances are strengthened because the easterly shear tends to trap waves in the lower troposphere. The upper-tropospheric disturbances can be reasonably assumed to propagate directly downward, thereby intensifying the lower-tropospheric disturbance. [Tam and Li \(2006\)](#) indicated the possible downward propagation of wave activity near 150°E, which is the longitude where the zonal wind shear between 200 and 850 hPa changes its sign. [Zhou and Wang \(2007\)](#) also proposed probable downward development in an unusual case when an upper-level MRG wave moved across the date line, where the prevailing vertical wind shear changed its sign. [Serra et al. \(2008\)](#) found downward energy propagation for a TD-type wave train from the middle to lower troposphere near the central equatorial Pacific. Other studies have also documented this downward propagation of upper-tropospheric disturbances near the central-western North Pacific ([Liebmann and Hendon 1990](#); [Dunkerton and Baldwin 1995](#); [Wu et al. 2015a](#)).

However, lower-level convergence and upper-level divergence would be created near the intersection of the easterly and westerly vertical shears. In addition to the trapping effect of the easterly shear, the low-level convergence would enhance low-level synoptic-scale waves by allowing wave energy to accumulate in the equatorial convergence zone ([Webster and Chang 1988](#); [Holland 1995](#); [Sobel and Bretherton 1999](#); [Kuo et al. 2001](#)) or to grow from the barotropic energy conversion because of the convergence and shear of the zonal mean flow ([Maloney and Hartmann 2001](#); [Wu et al. 2012](#); [Feng et al. 2014](#)). Therefore, the relative contributions of the direct downward transition of kinetic energy and the kinetic energy generation from the horizontal mean flow remain vague when an upper-level disturbance enters an easterly sheared environment from a westerly sheared

environment. Two hypotheses have been proposed for the role of this direct downward transition: 1) the downward propagation of kinetic energy directly enhances the low-level disturbance with comparable contribution to the low-level energy generation by the mean flow; and 2) the downward propagation only induces an enclosed low-level circulation, and further intensification should be attributed to other factors. Quantitative calculations should be conducted to determine the importance of downward transitions near critical longitudes.

This study aims to reveal the observational characteristics of TD-type waves affected by different sheared environments during the boreal summer over the western North Pacific and to investigate the physical mechanisms of wave growth and decay in complicated ambient flows associated with vertical wind shear. The rest of this paper is organized as follows: [section 2](#) describes the datasets used in this study, [section 3](#) reveals the observed characteristics of TD-type waves in different sheared background flows, [section 4](#) contains a discussion of the physical mechanisms based on an energetic diagnosis, and [section 5](#) presents conclusions and discussion.

2. Data and methodology

In this study, daily atmospheric fields on a global grid are obtained from the National Centers for Environmental Prediction–Department of Energy (NCEP–DOE) AMIP-II reanalysis ([Kanamitsu et al. 2002](#); [NCEP/NOAA/DOC 2000](#)) for June–November 1979–2013 and for the active seasons of tropical wave activity ([Frank and Roundy 2006](#); [Huang and Huang 2011](#)). The data have a spatial resolution of $2.5^\circ \times 2.5^\circ$, with 17 pressure levels. Outgoing longwave radiation (OLR) data from the Advanced Very High Resolution Radiometer sensors ([Liebmann and Smith 1996](#); [NOAA/OAR/ESRL/PSD 1996](#)) are obtained from the National Oceanic and Atmospheric Administration to provide deep convective information.

The wavenumber–frequency filtering method ([Wheeler and Kiladis 1999](#); [Schreck et al. 2011](#)) is used to extract signals of TD-type waves from the original fields. The filter is first applied using OLR to determine the most prominent mode of westward-propagating synoptic-scale waves over the western North Pacific. [Figure 1a](#) shows the resulting wavenumber–frequency spectra, including all wave bands, in the Northern Hemisphere from June to November for the 35 years. The filter captures the major peaks of each wave band, including the ER, MRG, Kelvin, and TD-type waves. Because ER waves possess a longer period and wavelength, the most prominent westward-propagating synoptic-scale waves

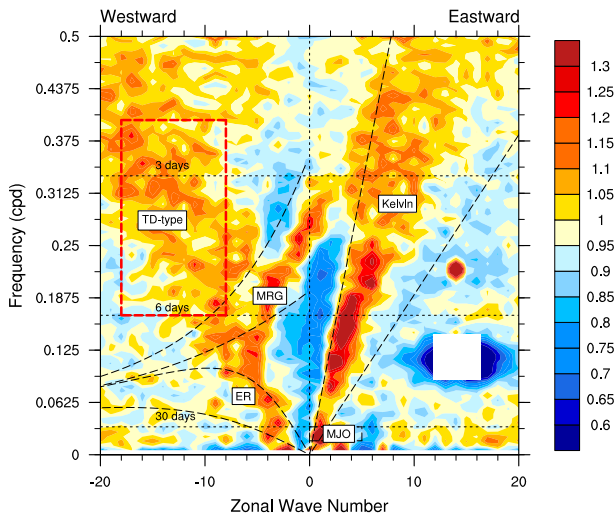


FIG. 1. Wavenumber–frequency spectrum of the OLR over the Northern Hemisphere from June to November 1979–2013. The filter band for TD-type waves is indicated by the red dashed rectangle.

are the MRG and TD-type waves. The wave bands of the MRG and TD-type waves are distinguishable by their dominant wavelengths and frequencies because TD-type waves have a relatively larger zonal wavenumber and higher frequencies than MRG waves. The separation of TD-type waves from MRG waves shows that the two wave types impact different regions in the western North Pacific. As shown in Fig. 2a, the OLR varies widely within the TD band throughout most of the tropical western North Pacific, with maxima appearing near 13°N , 140°E . In contrast, the OLR variance in the MRG waves is weaker than that in the TD-type waves and occurs mostly at lower latitudes, with the maxima near the central equatorial Pacific (not shown). This implies that MRG waves are constrained near the equator and occurred primarily farther east. In other words, MRG waves rarely propagate to the off-equatorial western Pacific. This might be attributed to the zonal standing of the precipitation associated with tropospheric MRG waves, as discussed in Kiladis et al. (2016). This proves that TD-type waves are the dominant synoptic-scale mode over the tropical western North Pacific during the boreal summer. Consequently, TD-type waves are selected as the typical mode for this study. The wavenumber–frequency band of a TD-type wave is determined over a period of 2.5–6 days, with negative zonal wavenumbers ranging from -8 to -18 , which capture the main peaks of high-frequency synoptic-scale fluctuations, as shown by the red rectangle in Fig. 1. Thereafter, the wavenumber–frequency filter is used for all atmospheric fields to regress the three-dimensional structure of TD-type waves. Next, a lagged-regression

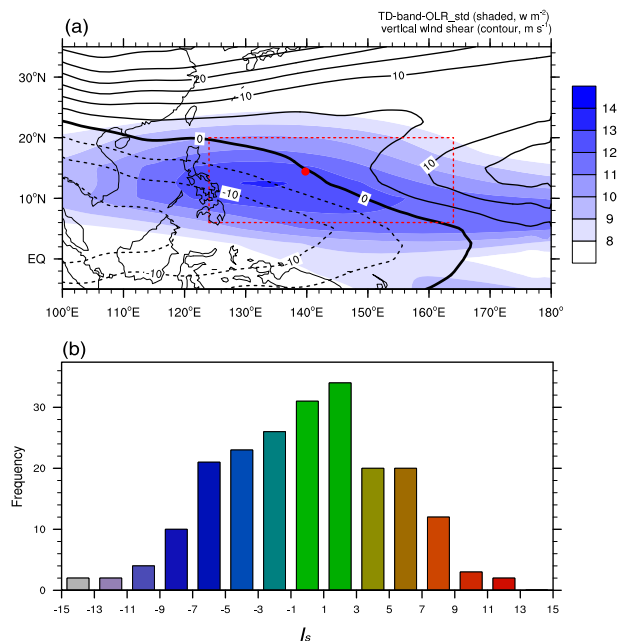


FIG. 2. (a) Climatology of the standard deviation of the TD-band OLR (shaded; W m^{-2}) and the vertical wind shear between 200 and 850 hPa (contours; m s^{-1}). The heavy black line denotes zero values for the vertical wind shear, and the dashed lines denote the negative values for the vertical wind shear. The red dashed rectangle denotes the critical region selected for calculating the wind shear index. The red dots denote the regression points. (b) Frequency histogram of the wind shear index.

analysis is used to reveal the evolution of a TD-type disturbance propagating westward from the westward sheared environment to the easterly sheared environment. In addition, a two-tailed Student's t test is used to estimate the statistical significance of the regressed fields, among which the degrees of freedom are reduced from the joint autocorrelation between the predictor and predictand following Livezey and Chen (1983). Finally, an eddy kinetic energy (EKE) budget equation, which is described in section 4, is derived to investigate the physical processes that govern wave growth/decay under different backgrounds.

It should be noted that the variance in the TD-band OLR is much larger than the variance in the MRG-band OLR in composition (not shown). The main reason is because the filter band for TD-type waves covers more bandwidth than that for MRG waves. Another possible reason is that the signals of tropical cyclones (TCs) embedded in the TD-band waves are not removed before filtering. However, previous studies have suggested that the variance of the TD-band waves is larger than that of the MRG band, even when the signals of tropical cyclones are removed (Schreck et al. 2011, 2012). Moreover, a TC-removing algorithm is tested in the

present research but makes little impact on the propagation and structure characteristics of the tropical waves, as stated by Xu et al. (2013). As a result, no TC-removing method is applied in this study.

3. Observed features

a. Vertically sheared background and wave activity

First, because vertical wind shear is closely related to horizontal mean flow, it is necessary to define typical circulation patterns associated with vertical wind shear during the boreal summer over the western North Pacific. Generally, zonal vertical wind shear is defined as the difference between zonal wind in the upper and lower pressure levels as follows:

$$S = U_{200} - U_{850}, \quad (1)$$

where U_{200} and U_{850} denote the zonal wind at 200 and 850 hPa, respectively. Regions with $S > 0$ feature westerly shear, and regions with $S < 0$ feature easterly shear. The climatology of vertical wind shear during boreal summer is illustrated in Fig. 2a, which shows a northwest–southeast orientation. The zero line of the vertical wind shear extends southeastward from the South China Sea to the equatorial central Pacific and separates the western North Pacific into two areas based on the sign of the vertical wind shear. Easterly shear occurs in the southwestern part of the Pacific Ocean, and westerly shear occurs in the northeastern part of the Pacific Ocean. Furthermore, Fig. 2a shows that the TD-band waves are active near the weak easterly sheared region.

By considering the wave activity and the distribution of vertical wind shear, an index representing the environmental conditions of vertical wind shear is defined as follows:

$$I_s = \frac{1}{J} \frac{1}{I} \sum_{j=1}^J \sum_{i=1}^I \overline{S_{ij}} \quad \left(\begin{array}{l} i = 1, 2, \dots, I \\ j = 1, 2, \dots, J \end{array} \right). \quad (2)$$

In Eq. (2), S_{ij} is the vertical wind shear at a certain grid point (i, j) inside the region of 6° – 20° N, 124° – 164° E (the region outlined by red dashes), and an overbar denotes the monthly mean. Therefore, the index I_s expresses the monthly and regionally averaged zonal wind shear between 200 and 850 hPa. No standardization is applied to the index because the vertical wind shear traps waves at the upper or lower levels as a result of the sign of the vertical wind shear, rather than the sign of the vertical shear anomaly. Thus, the monthly averaged circulation corresponding to the vertical wind shear is considered a background condition that varies slowly and affects tropical TD-type waves.

The statistical distribution of I_s during each June–November from 1979 to 2013 is shown in Fig. 2b. The results show an approximately normal distribution. The I_s indices for most months are between -7 and 7 m s^{-1} . To acquire a sufficient number of representative samples for further study, cases with I_s values less than -5 m s^{-1} and greater than $+5 \text{ m s}^{-1}$ are assigned to easterly shear and westerly shear, respectively. Consequently, 39 months are selected in the easterly shear category, and 37 months are selected in the westerly shear category, accounting for 18.6% and 17.6% of the total samples, respectively. In addition, cases with I_s indices between -1 and $+1 \text{ m s}^{-1}$ are also selected and represent 31 months (14.8%). As discussed below, these cases show a transition pattern in which the easterly shear gradually changes to westerly shear with increasing longitude. Therefore, this category is called the shear transition. Additional analyses suggest the remaining cases, with I_s indices between -5 and -1 m s^{-1} or $+1$ and $+5 \text{ m s}^{-1}$, also show transition patterns but at different critical longitude (not shown). As Table 1 shows, the easterly sheared cases mostly occur in July to October; the westerly sheared cases mostly occur in June, July, October, and November; and the transition cases occur throughout the entire period. This implies a potential influence of the seasonal cycle on the following results. Although the current composite method cannot exclude the impact of the seasonal cycle on wave characteristics, the major results can be tested by applying the same composition for each month, thereby reducing the impact of the seasonal cycle. This test shows that the major results of the separate-month test are generally consistent with those for the entire period (not shown). This demonstrates that the major findings in our manuscript are robust, even though the impact of the seasonal cycle is included in the composition.

Figure 3 shows the composite patterns of the vertical wind shear, the 850-hPa horizontal wind, and the standard deviation of the TD-band-filtered OLR. In the easterly shear category, the negative value of the vertical wind shear dominates the tropical western North Pacific (Fig. 3a). The maximum standard deviation of the TD-band-filtered OLR occurs near 14° N, 135° E, and the wave activity is mostly affected by the easterly sheared environment. In the westerly shear category, the western North Pacific is governed by positive vertical wind shear, and the region with active TD-type waves is located near the moderate wind shear between -5 and $+5 \text{ m s}^{-1}$ (Fig. 3b). In the shear transition pattern, the I_s index in the critical region is near zero, and the composite results (Fig. 3b) are similar to the climatology results (Fig. 2a). The shear transition pattern consists of two equally split sections, with

TABLE 1. Monthly distribution of selected cases.

	Total	Jun	Jul	Aug	Sep	Oct	Nov
Easterly shear	39	0	5	19	11	4	0
Westerly shear	37	11	2	0	0	4	20
Shear transition	31	6	10	3	4	7	1

westerly shear in the northeast and easterly shear in the southwest. Thus, the shear transition category is used to study the evolution of the TD-type waves propagating from the westerly sheared environment to the easterly sheared environment. As shown in Figs. 3a and 3b, the spatial span and perturbation intensity in the westerly shear are smaller and weaker than the span and intensity in the easterly shear.

b. Three-dimensional structure

1) HORIZONTAL STRUCTURE

To reveal the three-dimensional characteristics of the TD-type waves under different vertically sheared large-scale flows, atmospheric variables are regressed based on the time series of the TD-band-filtered OLR at 15°N, 140°E (the red dot shown in Fig. 2a). Additional examinations based on other regression points (e.g., the variance maxima of the TD-band OLR and the central point of the critical region) show that the results are not sensitive to the selection of the regression point.

The horizontal patterns of the TD-type wave at 200 and 850 hPa are shown in Fig. 4. Affected by easterly sheared environment, the TD-type wave is characterized by alternating convergent–divergent–convergent perturbations in the upper troposphere (Fig. 4a), a well-organized northwest–southeast wave train in the lower troposphere (Fig. 4c), and coupled suppressed–enhanced–suppressed convections patterns. Notably, the upper-level perturbations feature neither enclosed circulations nor rotated wind fields with well-organized structure. Thus, they should be regarded as convergent–divergent–convergent perturbations other than a Rossby wave train. These divergent (convergent) centers coincide with enhanced (suppressed) convections. Comparatively, in the westerly sheared background, the most distinctive feature is the well-organized upper-tropospheric wave train with alternating anticyclonic–cyclonic–anticyclonic disturbances (Fig. 4b). However, the low-level disturbances are relatively weaker in the westerly sheared background than in the easterly sheared background (Fig. 4d). Moreover, the upper-level disturbances are located nearly 10° northwest of their low-level counterparts. Consequently, the upper-level cyclonic (anticyclonic) disturbances lead enhanced (suppressed) convections

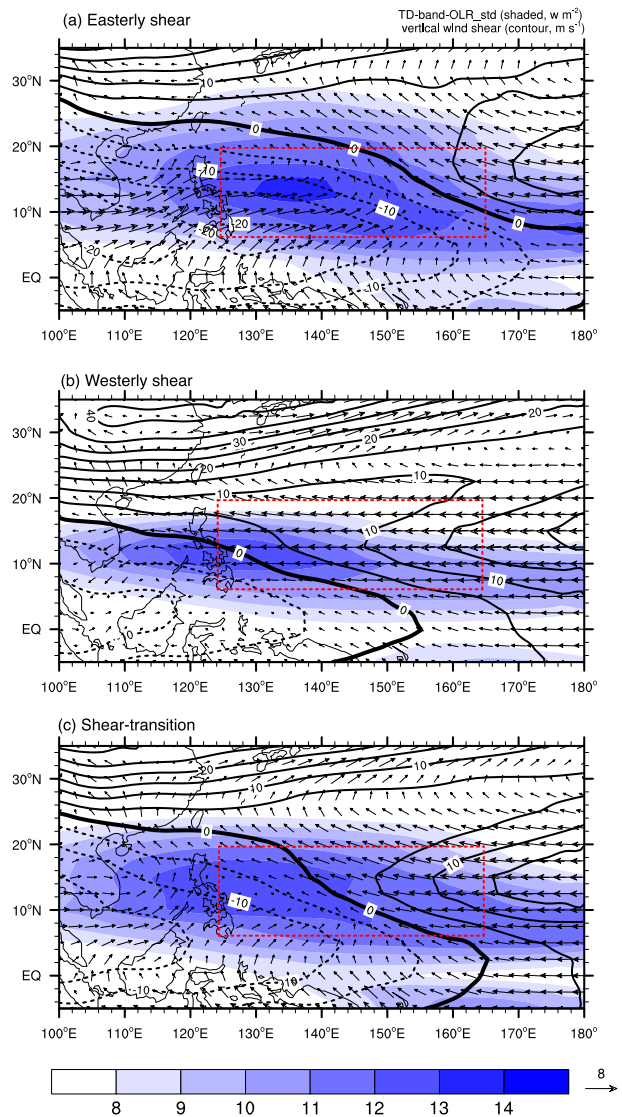


FIG. 3. Horizontal wind at 850 hPa (vectors), the standard deviation of the TD-band OLR (shaded; W m^{-2}), and the vertical wind shear between 200 and 850 hPa (contours; m s^{-1}) in (a) the easterly sheared, (b) the westerly sheared, and (c) the shear transition categories. The heavy black line denotes the zero values for the vertical wind shear, and the dashed lines denote negative values for the vertical wind shear. The red dashed rectangle denotes the critical region selected for calculating the wind shear index.

by approximately one-quarter of a wavelength, and the low-level vortices approximately coincide with the convections. Furthermore, the low-level disturbances can be traced back to the ocean near 160°E, regardless of their background flows. However, the upper-tropospheric waves in the westerly sheared flows can be traced back to the eastern Pacific (Fig. 4b), and no wave train is observed in the upper troposphere near the central Pacific under the easterly sheared flow.

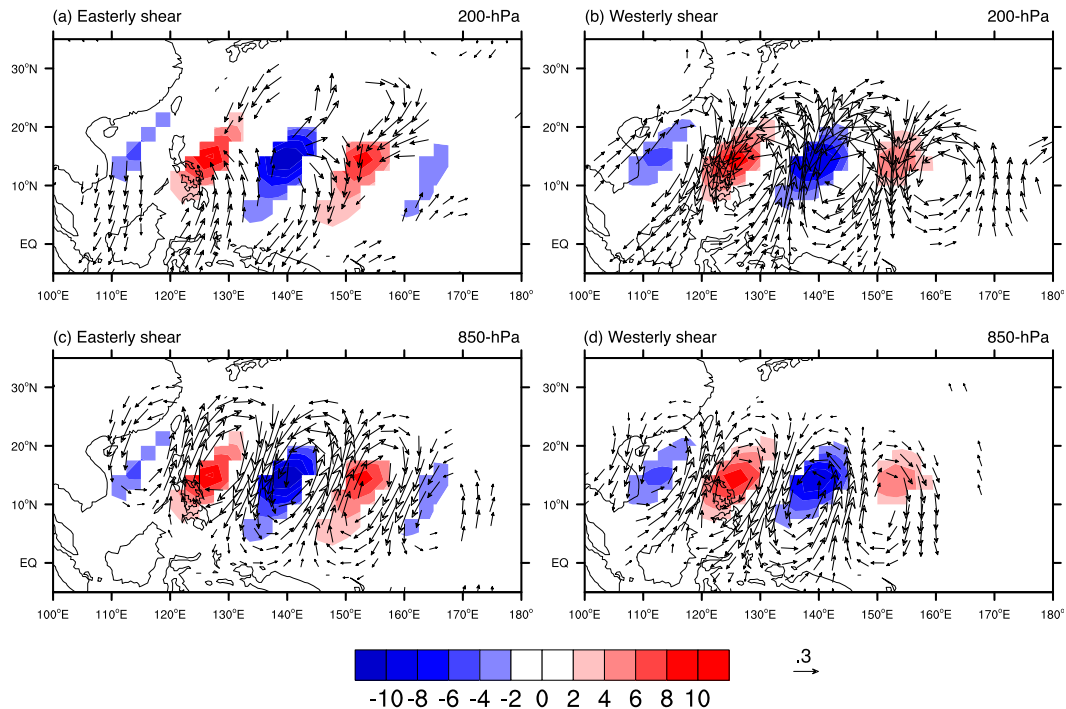


FIG. 4. Regressed OLR (shaded; $W m^{-2}$) and horizontal wind (vectors) at (a) 200 hPa in the easterly sheared category, (b) 200 hPa in the westerly sheared category, (c) 850 hPa in the easterly sheared category, and (d) 850 hPa in the westerly sheared category. The regression is based on the filtered OLR at $15^{\circ}N, 140^{\circ}E$. Only fields exceeding the 95% confidence level are shown.

2) VERTICAL STRUCTURE

As shown in Fig. 4, the upper-tropospheric waves differ under different sheared environments. Detailed vertical structures obtained by averaging the latitude belt from 10° to $20^{\circ}N$ are shown in Fig. 5. Figures 5a and 5c show the vertical structures of the meridional wind, relative vorticity, temperature, and vertical pressure velocity associated with the TD-type waves under easterly sheared ambient flow. The regressed relative vorticity and meridional wind show nearly equivalent barotropic structures with a slight westward tilt. Fluctuations are generally observed in the lower and middle troposphere, with a maximum at approximately 400–500 hPa, as shown in Fig. 5a. Regarding the temperature anomaly and vertical pressure velocity, both maxima occur in the middle-upper troposphere, as shown in Fig. 5c. Warm anomalies correspond to upward motion, and cold anomalies correspond to downward motion. Nonnegligible cold anomalies are found above and below the midlevel warm core in a TD-type disturbance near $140^{\circ}E$, which has been documented by many observational studies (e.g., Chang et al. 1970; Tam and Li 2006). Interestingly, a clear eastward tilt with height is present in the vertical pressure velocity.

Consequently, the maximum temperature and vertical velocity are not perfectly matched. As shown in Fig. 5c, a phase difference of approximately one-eighth occurs between the vertical velocity and the temperature anomaly at 300 hPa. A lead-lag analysis also reveals this phase difference (not shown). Additionally, because of the complex structure of the upper-level perturbations (Fig. 4a), vertical slices along other latitudes (e.g., along 8° – $10^{\circ}N$ or 20° – $22^{\circ}N$) are also produced. The major features are similar to those averaged between 10° and $20^{\circ}N$ (Figs. 5a,c): for example, a westward-tilted vertical structure, maximum meridional wind near 500 hPa, less-organized upper-level structure, and eastward-tilted vertical motion.

The vertical structure of the TD-type wave is discriminative in the westerly sheared environment. Figure 5b shows upper-tropospheric fluctuations with a maximum at 200 hPa. The meridional wind and relative vorticity both show a vertical structure with a remarkable westward tilt extending from the sea surface layer to the tropopause. To the east of $150^{\circ}E$, the disturbances are confined in the upper troposphere, and the low-level perturbations are weak. However, to the west of $150^{\circ}E$, lower-troposphere disturbances have slightly larger amplitude. Nevertheless, the upper-level disturbance can

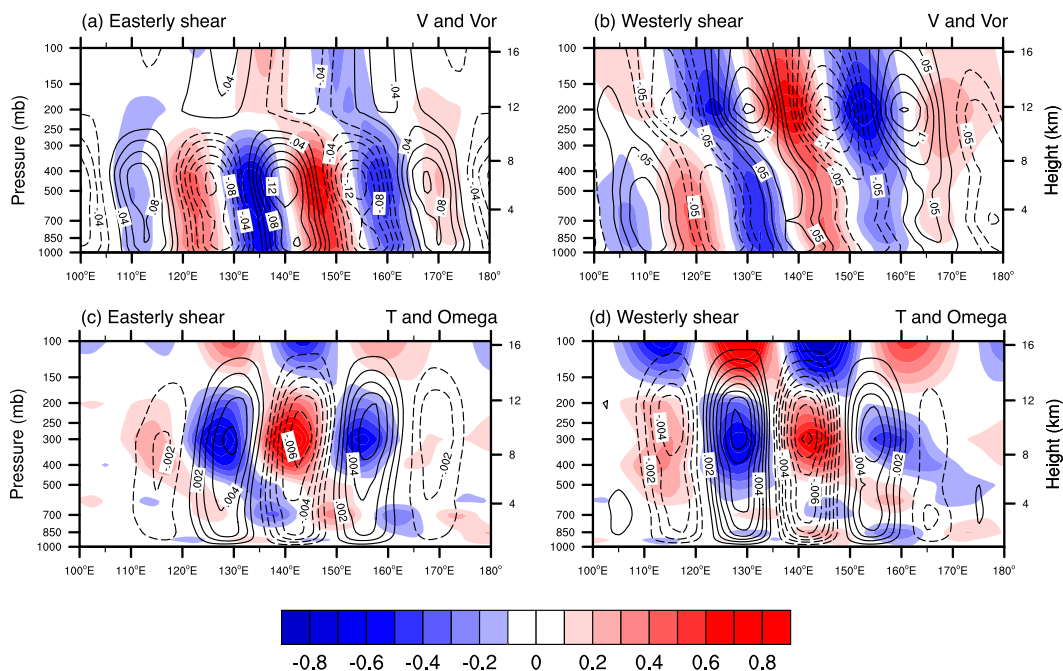


FIG. 5. Longitude–height plot of the regressed meridional wind (shaded; m s^{-1}) and the relative vorticity (contours; 10^{-6} s^{-1}) averaged between 10° and 20°N in the (a) easterly sheared and (b) westerly sheared categories and the longitude–height plot of the regressed vertical pressure velocity (contours; Pa s^{-1}) and temperature (shaded; 10^1 K) in the (c) easterly sheared and (d) westerly sheared categories. The regression is based on filtered OLR at 15°N , 140°E .

still be identified near 120°E based on its prominent vorticity perturbation at 200 hPa. Unlike the tilted structures of the relative vorticity and meridional wind, the vertical pressure velocity is less tilted, as shown in Fig. 5d. The maximum vertical velocity appears near 250 hPa, which indicates an in-phase relationship with the temperature maxima. The upward motions are well matched with warm perturbations, and the downward motions are well matched with cold anomalies.

Upward motion inside a warm region implies a conversion from eddy available potential energy (EAPE) to EKE. The wave structures in the easterly shear and westerly shear both support this energy conversion. This suggests that the conversion from EAPE to EKE is an important energy source for the Pacific TD-type waves, which supports the findings of previous studies (Tai and Ogura 1987; Lau and Lau 1992; Serra et al. 2008). However, comparing Figs. 5c and 5d, the upward motion in the easterly sheared environment is weaker than that in the westerly sheared environment. Moreover, the phase difference between vertical velocity and temperature in the middle troposphere induced by the eastward tilt of vertical velocity is also an important factor affecting wave energy conversion. This will be discussed in detail in section 4. On the other hand, in the easterly sheared environment, the structure of these waves

indicates a positive feedback between deep convection and synoptic-scale waves, which falls under the “moisture mode” concept (Mapes 2000; Sobel et al. 2001; Raymond and Fuchs 2007) or the “wave CISK” framework (Hayashi 1970; Lindzen 1974; Davies 1979). Both of these two frameworks suggest that the upward motion possess a phase tilt with height with respect to the propagation direction, thus forming a phase difference between the upward motion and the diabatic heating if a positive feedback exists between convective heating and circulation (Bolton 1980; Zhang and Geller 1994; Raymond and Fuchs 2007). As Fig. 5c shows, the eastward tilt in the vertical velocity induces a phase lag with the convection (maximum convection is centered at 140°E as well as the regression point) in the easterly shear. This means that the convection and circulation are more tightly coupled in the easterly sheared environment and favor wave growth through wave–convection feedback. However, in westerly shear, the vertical motions are straight upward or downward. Thus, this positive feedback between convection and circulation may not exist for the waves in the westerly sheared environment.

The vertical structure of the synoptic-scale disturbances below 250 hPa in the easterly sheared environments is similar to that of the TD-type waves reported in previous studies (Reed and Recker 1971; Takayabu

and Nitta 1993; Serra et al. 2008). However, the upper-level structure is somewhat obscure in the present composition. Previous studies suggested the TD-type disturbance possesses an upper-level counterpart with secondary maxima near 200 hPa. Figure 4a indicates that upper-level disturbance is less rotated. We suspect that this is due to the extreme easterly sheared cases selected in the composition; thus, strong deep convection may induce upper-level perturbations in association with the inertial-gravity wave (Lane et al. 2001). Tam and Li (2006) showed that temperature anomalies mainly occur in the upper and lower troposphere. However, current results suggest that the temperature anomalies of a TD-type wave are observed near 250 or 300 hPa, as suggested by Lau and Lau (1990), regardless of the circulation background.

c. Wave evolution while traversing westerly and easterly sheared environments

The above results indicate that synoptic-scale waves are sensitive to the local vertical shear over the western North Pacific. Because the climatological vertical wind shear always spreads northwest–southeast over the western North Pacific (Fig. 3c), a westward-propagating wave will move from the westerly sheared environment to the easterly sheared environment. Thus, the systematic changes in a TD-type disturbance crossing the critical longitude dividing the easterly and westerly sheared areas are investigated using a lagged-regression method.

When westward-moving disturbances cross the critical longitude (approximately 140°E) they are affected by easterly sheared basic flow. Otherwise, the westward-moving disturbances are influenced by the westerly sheared background. Figure 6 shows the evolution of synoptic-scale disturbance with the maximum in the upper troposphere penetrating an easterly sheared environment from a westerly sheared background. Three days before day 0, a well-organized low-level wave train exists in a northwest–southeast orientation (Fig. 6a). The cyclonic disturbance near 8°N, 155°E (marked as A) shows that the wind fields exhibit a slight eastward tilt with increasing latitude. This implies that the wave is barotropically unstable and will develop by extracting kinetic energy from the basic state. The low-level disturbance is coupled with enhanced convective activity (marked as C) in the northeastern quadrant of cyclone A. Meanwhile, an east–west-oriented wave train with larger wind perturbations emerges at 200 hPa (Fig. 6b). Because of the vertical structure of the westward tilt with height under the westerly sheared basic flows, a phase difference between the convection C and the upper-level vortex B is approximately in quadrature. Thus, the upper-level disturbance B is located approximately 500 km northwest of

the low-level disturbance A. While the disturbance propagates westward, the low-level disturbance gradually becomes more intense and shifts slightly poleward on day 0 (Fig. 6c). Consequently, the convection and circulation become closer and have nearly coinciding phases. Meanwhile, the upper-level disturbance B moves to nearly 130°E without significant intensification (Fig. 6d). The regression results show a slight equatorward shift in the upper-level disturbance B, rather than poleward migration. Consequently, the lower-level disturbance becomes more vertically coupled with its upper-level anticyclonic counterpart following B. Three days later (a lag of +3 days), the low-level disturbance A further develops, migrates northwestward, and tilts more eastward with latitude (Fig. 6e). In the upper troposphere, the disturbance has already dissipated; thus, no notable organized vortex can be identified over the South China Sea (Fig. 6f). Simultaneously, the low-level vortex center A lags behind the OLR anomaly C by a phase difference of approximately one-eighth.

The results suggest there are systematic relative motions between low-level disturbances and convections. The enhanced convection lags behind the accompanying low-level cyclonic disturbance by approximately one-eighth of a wavelength near 160°E but leads the low-level disturbance by approximately one-eighth of a wavelength to the west of 140°E. This is similar to the composition results for the easterly and westerly cases (Figs. 4c,d). This suggests that the relative positions of convections and circulations are closely related to the vertical wind shear. Previous studies have also found that the precipitation shifts from slightly east of the low-level disturbance in the central Pacific to west of the low-level disturbance farther west (Reed and Recker 1971; Tam and Li 2006; Serra et al. 2008). The current results are consistent with the theoretical study by Holton (1971).

Figure 7 shows the systematic evolution of the vertical structure of a westward-propagating upper-tropospheric disturbance. The lower-tropospheric disturbance A and upper-tropospheric disturbance B are also identified in Fig. 6. Three days before day 0, the disturbance shows a representative upper-level fluctuating mode, while the lower-level perturbations are relatively weak (Fig. 7a). The upper- and lower-level disturbances both show a westward-tilted structure, which implies that developments have occurred in both levels. As will be revealed later, this development is attributed to upper- and lower-level troughs. Meanwhile, corresponding upward motion (marked as D) is observed near 158°E, with some eastward tilting with height (Fig. 7b). The mid-level warming (marked as C) appears approximately 10° east of the anomalous upward motion (D). On day 0, the maximum meridional wind surrounding the

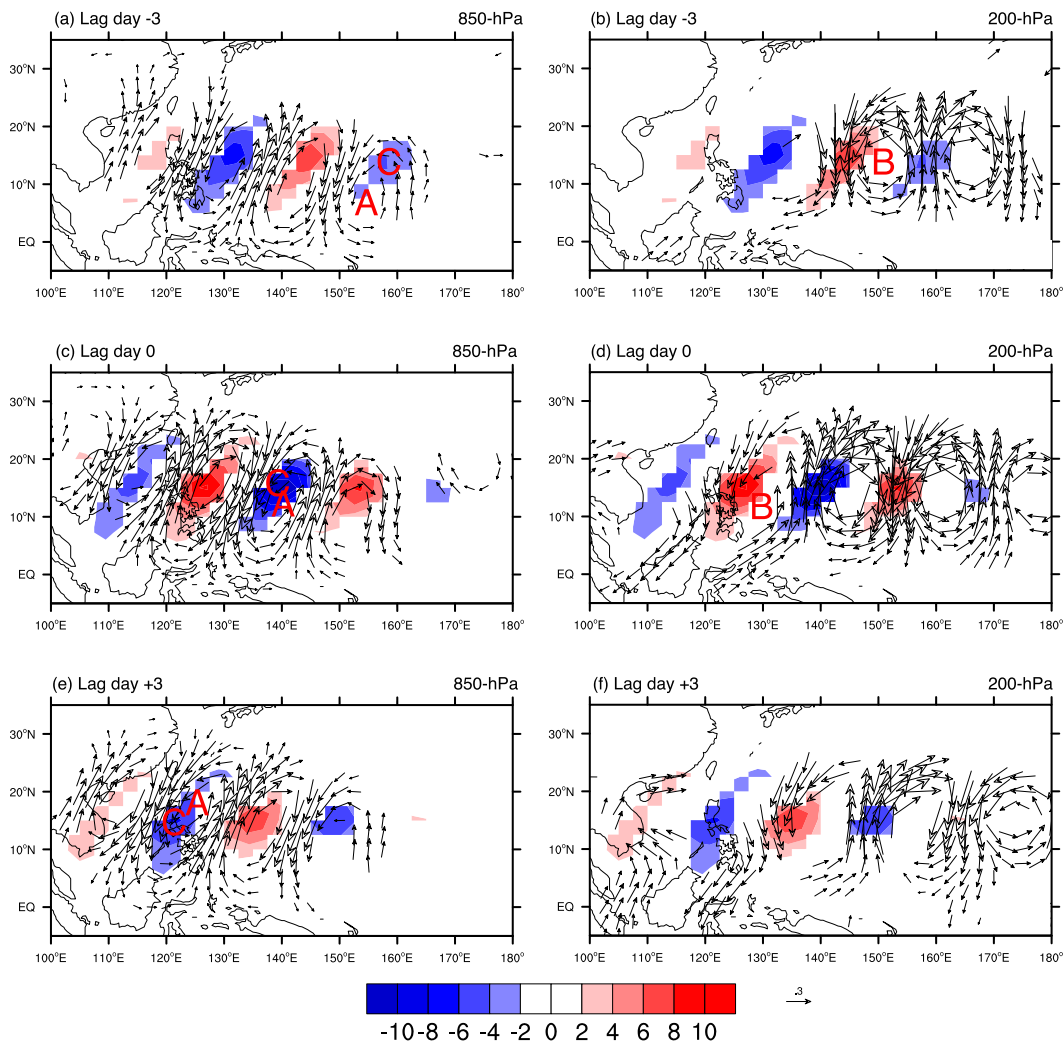


FIG. 6. Regressed OLR (shaded; W m^{-2}) and horizontal wind (vectors) in the shear transition category at 850 hPa on lag days (a) -3 , (c) 0 , and (e) $+3$ and at 200 hPa on lag days (b) -3 , (d) 0 , and (f) $+3$. The regression is based on the filtered OLR at 15°N , 140°E . Only fields exceeding the 95% confidence level are shown. The markings A, B, and C denote the vortex center at 850 hPa, the vortex center at 200 hPa, and the convection center, respectively.

low-level vortex A significantly increases from approximately 0.2 m s^{-1} (Fig. 7a) to more than 0.6 m s^{-1} (Fig. 7c) near 850 hPa. Additionally, the relative vorticity also increases. Nevertheless, the upper-level vortex B becomes straight vertical and slightly weaker than three days before day 0. The vertical pressure velocity (D) and midtropospheric temperature (C) anomaly both become more intense and nearly in-phase with the low-level vortex (Fig. 7d). The upward motion of warm air and downward motion of cold air implies the conversion from EAPE to EKE. As the disturbance moves farther westward, the upper-level vortex rapidly dissipates, and the low-level vortex becomes stronger. Then a low-level disturbance further develops with a maximum

at 850 hPa and a secondary maximum at 500 hPa (Fig. 7e). This disturbance is vertically coupled with an upper-level perturbation with the opposite phase. However, the upper-level structure above 250 hPa becomes eastward tilted, and its maximum is outside of the troposphere. Later, the midtropospheric warming (C) leads the upward motion (D) by nearly one-eighth of a wavelength after $+3$ lag days (Fig. 7f). This implies that the disturbance is conditionally unstable and can develop through the convection–circulation feedback, as discussed above.

The evolution of the horizontal and vertical structures in a wave disturbance in the transition case can be similarly represented by the typical characteristics from the westerly sheared environment to the easterly sheared

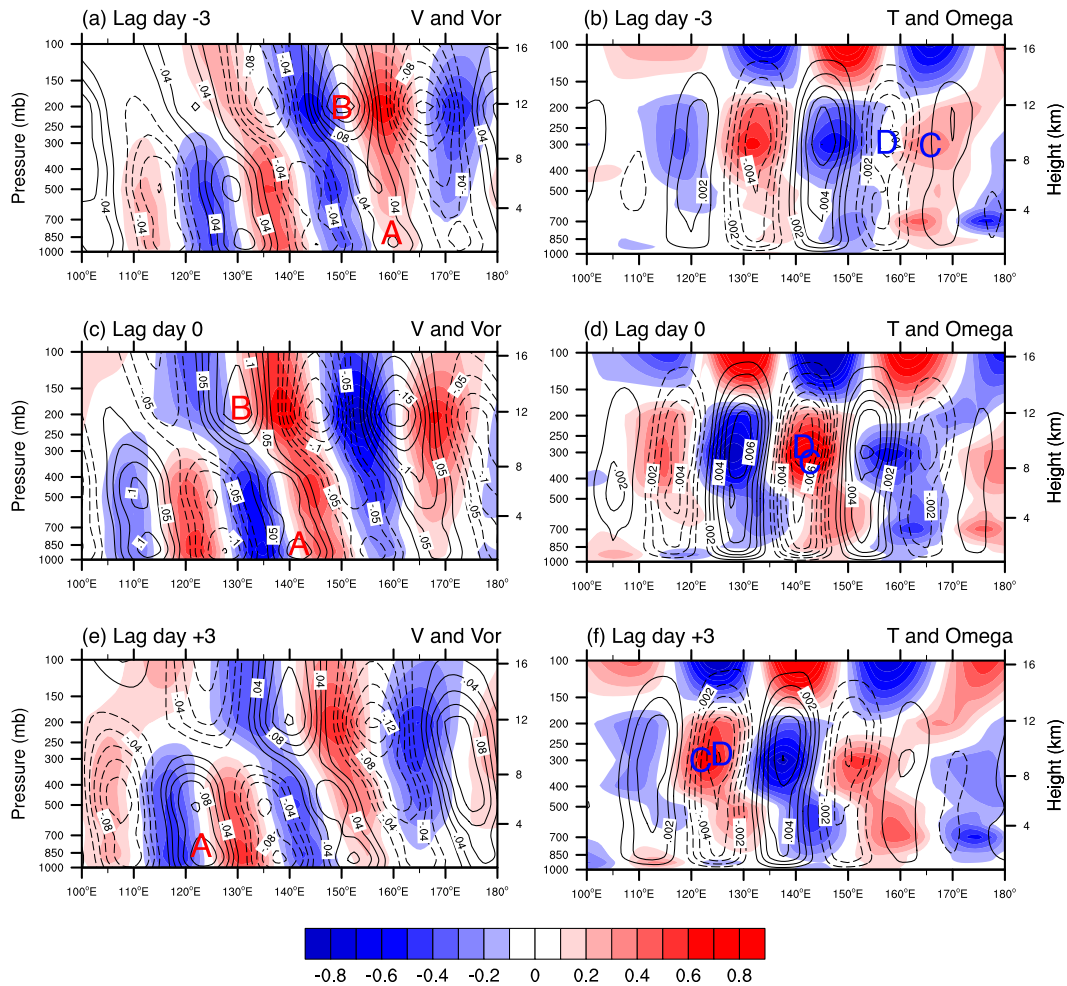


FIG. 7. Longitude–height plot of the regressed meridional wind (shaded; m s^{-1}) and relative vorticity (contours; 10^{-6} s^{-1}) averaged between 10° and 20°N on lag days (a) -3 , (c) 0 , and (e) $+3$, and the longitude–height plot of the regressed vertical pressure velocity (contours; Pa s^{-1}) and temperature (shaded; 10^1 K) on lag days (b) -3 , (d) 0 , and (f) $+3$ in the shear transition category. The regression is based on the filtered OLR at 15°N , 140°E . The markings A, B, C, and D denote the vortex center at 850 hPa, the vortex center at 200 hPa, the temperature perturbation, and the vertical velocity perturbation, respectively.

environment. The only difference is that the vertical velocity is straight vertical in the composition for westerly cases but is eastward tilted throughout the entire period in this lead–lag regression. Some inconsistencies exist in the vertical structure of the vertical velocity of a TD-type disturbance among the different observational studies. For example, Takayabu and Nitta (1993) showed that the vertical velocity is less tilted in their compositions, and they suggested that the wave-CISK mechanism is not the significant mechanism for TD-type waves. However, Tam and Li (2006) showed that the vertical motion of TD-type waves is slightly eastward tilted in the western North Pacific; thus, it exhibits a phase difference between the vertical motion and relative vorticity (in their Fig. 8a). More investigation is needed on this issue.

The horizontal wind and EKE, which is defined as $K' = 1/2(u'^2 + v'^2)$, are averaged inside a $10^\circ \times 10^\circ$ box centered at the disturbance center (following A in Figs. 6a,c,e) at 850 hPa. Thus, a time–height diagram can be used to investigate the EKE change while the disturbance intrudes into an easterly sheared background from a westerly sheared background, as shown in Fig. 8. The development in the upper troposphere begins on lag day -5 and reaches its maximum on lag day -1 . Meanwhile, the vertical wind shear becomes negative, which indicates that the disturbance has already penetrated the easterly sheared flows at lag day -1 (Fig. 8c). Simultaneously, the meridional wind and EKE both show downward transitions from the upper troposphere to the middle troposphere

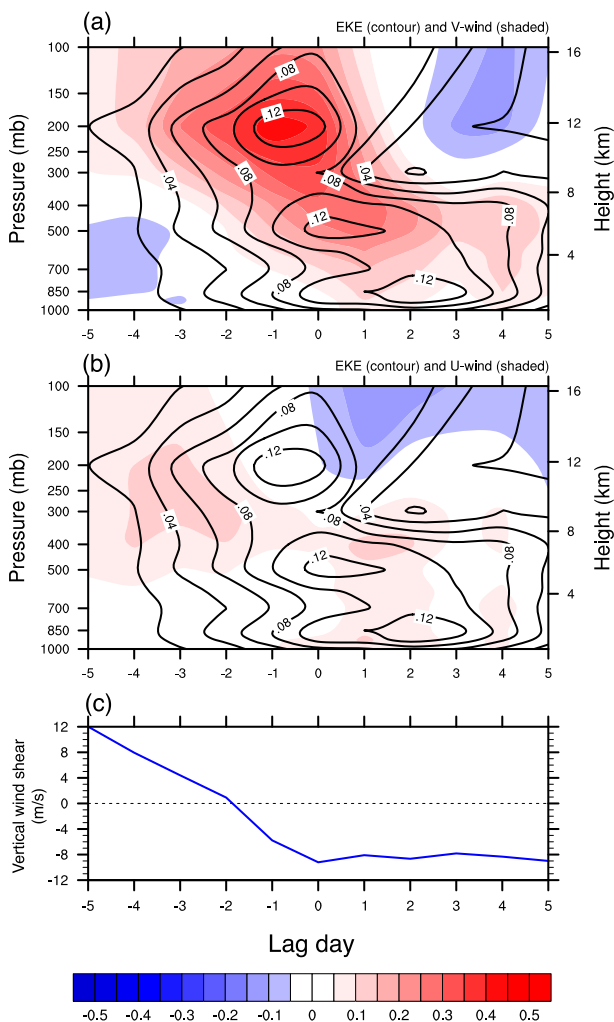


FIG. 8. Time–height plot of the (a) EKE (contours; $\text{m}^2 \text{s}^{-2}$) and meridional wind (shaded; m s^{-1}), (b) EKE (contours; $\text{m}^2 \text{s}^{-2}$) and zonal wind (shaded; m s^{-1}), and (c) vertical wind shear (m s^{-1}) averaged for the $10^\circ \times 10^\circ$ rectangle with the center at the vortex center at 850 hPa. The horizontal coordinates are the lag days.

(Fig. 8a), as suggested in previous studies (Tam and Li 2006; Serra et al. 2008). After day 0, the upper-level disturbance weakens significantly. Nevertheless, while the upper-level EKE begins to transition downward at approximately day 0, the zonal wind component and EKE independently increase in the middle and lower troposphere (Fig. 8b). However, the meridional wind does not show such changes (Fig. 8a). The different signals between the zonal and horizontal wind components can also be found in the results of Dunkerton and Baldwin (1995, in their Fig. 7), despite their focus on the MRG waves over the central-eastern Pacific. Consequently, the downward transport of momentum and kinetic energy occurs as the upper-level disturbance penetrates the

easterly sheared background from the westerly sheared background. However, different processes are likely responsible for the developments in the middle and lower troposphere, respectively.

It should be noted that Serra et al. (2008) illustrated upward phase propagation and downward energy dispersion of westward-propagating TD-type waves in their lead–lag compositions at Majuro (7.1°N , 171.4°E ; see their Fig. 11b). By using the bandwidth of the filter similar to Serra et al. (2008), this downward energy propagation can be well reproduced over the central Pacific despite some differences in detail. However, the signal of downward energy dispersion is not found over the western North Pacific, even though a broader filter band is applied (not shown). Thus, the current downward transition might not be explained by the vertical propagation of TD-type waves. To investigate the mechanisms of the middle and lower developments and the role of the vertical transport of EKE, quantitative calculations and discussions are conducted in the next section.

4. Possible mechanisms

In general, TD-type waves are westward-propagating Rossby waves over the tropical ocean. These waves can be destabilized by large-scale basic flows with horizontal shear or vertical shear (Holton 2004). In theory, a westward-propagating TD-type wave is strengthened near regimes with horizontally sheared basic flows where the absolute vorticity of the basic flow is at a minimum or a maximum through barotropic instability (Boyd 1978a,b). On the other hand, a moderate vertical wind shear is favorable for destabilizing a Rossby wave through baroclinic instability, which favors the transformation of mean available potential energy (MAPE) to EAPE (Xie and Wang 1996). In this section, an energetic diagnosis is adopted to investigate the physical mechanisms of the effects of vertical wind shear on TD-type waves.

a. Source of eddy kinetic energy

Despite the potential for some inconsistencies in the energy budget calculations associated with the use of different reanalysis datasets, energetic diagnoses have been widely used to investigate the dynamic processes of wave growth and decay (Lau and Lau 1992; Chen and Huang 2009; Wu et al. 2014, 2015b). In this section, an EKE budget equation is derived following the work of Lau and Lau (1992) and Chen and Sui (2010). The EKE tendency in a three-dimensional atmosphere can be written as follows:

$$\begin{aligned} \frac{\overline{\partial K'}}{\partial t} = & -\overline{V'_h \cdot (V' \cdot \nabla) V_{h \text{ basic}}} - \frac{R}{P} \overline{\omega' T'} - \overline{V' \cdot \nabla \Phi'} \\ & - (V_{h \text{ basic}} \cdot \nabla_h \overline{K'} + \overline{V'_h \cdot \nabla_h K'}) \\ & - \left(\omega_{\text{basic}} \frac{\overline{\partial K'}}{\partial z} + \overline{\omega' \frac{\partial K'}{\partial z}} \right) + D. \end{aligned} \quad (3)$$

In Eq. (3), K' represents the horizontal EKE, the overbars denote time-averaged values, the subscript h indicates horizontal components, the subscript “basic” indicates the basic field averaged for different cases, and a prime symbol indicates the regressed fields obtained by projecting the data onto the TD-filtered OLR in section 3. The other symbols follow conventional definitions. The first term on the right-hand side is the barotropic conversion term, which represents the effects of horizontal mean flow on eddy fluctuations by converting time-mean kinetic energy (MKE) to EKE. The second term represents the conversion of energy from EAPE to EKE. The third term is the effect of the local convergence of eddy geopotential flux. The fourth term is the horizontal transport, and the fifth term is the vertical transport. The last term is the dissipation term, which is affected by friction and other subgrid-scale effects. The first two terms are the sources or sinks for EKE growth and decay, terms three, four, and five describe the redistribution of EKE, and the last term is another sink for EKE.

The sources of EKE that affect growth and decay are investigated in this section. Figure 9 shows a longitudinal–height plot of the first two terms in Eq. (3) along the axis of the wave trains averaged from lag day -5 to lag day $+5$. As shown in Fig. 9a, in an easterly sheared basic flow, EKE growth occurs near 850 hPa, spreading from 115° to 150°E . Above 500 hPa, a negative value indicates that upper-level disturbances are weakened by the horizontal mean flow. Thus, the horizontal mean flow associated with the easterly sheared background favors wave growth in the lower troposphere, which is generally consistent with the observed structure of the EKE distribution. However, in the westerly sheared basic flow (Fig. 9c), EKE growth and decay are both found in the upper troposphere near 200 hPa, with positive values found east of 140°E and negative values found west of 140°E . Considering that the disturbances move westward, this result is also consistent with the observed EKE. Because the circulation background for shear transition cases could be considered a combination of westerly sheared basic flow in the northeast and easterly sheared basic flow in the southwest, the EKE distributions and the EKE tendencies exhibit interesting features. Figure 9e shows upper-level growth east of 140°E , which is consistent with the upper-tropospheric EKE maxima, and lower-level growth west

of 140°E , which is consistent with the lower-tropospheric EKE maxima. Thus, while an easterly (westerly) shear confines the disturbance to the lower (upper) troposphere, the wave growth induced by horizontal mean flow also occurs in the lower (upper) troposphere.

Conversion from EAPE to EKE is ascribed to the upward motion of warm air and downward motion of cold air, as the second term of Eq. (3) indicates. As shown in Figs. 9b, 9d, and 9f, the value of EKE converted from EAPE is several times larger than the barotropic conversions, indicating that the conversion from EAPE to EKE is more important than barotropic conversions for TD-type waves. In the easterly shear, the transition from EAPE to EKE is slightly smaller than in the other two basic flows. As shown in Eq. (3), the conversion from EAPE to EKE is inversely proportional to the production of transient vertical pressure velocity and temperature anomalies. Smaller transition rates from EAPE to EKE in the easterly shear could be ascribed to the smaller vertical velocity and the critical phase difference between the vertical velocity and temperature anomaly at the intermediate level (Fig. 5c), which leads to the extraction of less EKE from EAPE. As in Serra et al. (2008), the conversion from EAPE to EKE occurs near the middle to upper troposphere, roughly from 400 to 150 hPa, regardless of the circulation background. This is due to the physical limitations on the vertical distributions of temperature and ω . Regardless, the current composition suggests that the transition from EAPE to EKE is less correlated with the EKE distribution and is less responsible for EKE growth in the upper or lower troposphere.

b. Barotropic energy conversions

As mentioned above, the barotropic conversion is the critical source of kinetic energy responsible for wave growth at different levels in association with different sheared environments. Thus, the barotropic energy conversion is further examined to investigate how the horizontal mean flow affects the wave growth.

Barotropic energy conversions can be explained by the shear and convergence of the horizontal mean flow. The expansion of the barotropic energy conversion term in Eq. (3) can be written as follows:

$$\frac{\overline{\partial K'_{\text{baro}}}}{\partial t} = -\overline{u'v'} \frac{\partial \bar{u}}{\partial y} - \overline{u'v'} \frac{\partial \bar{v}}{\partial x} - \overline{u'^2} \frac{\partial \bar{u}}{\partial x} - \overline{v'^2} \frac{\partial \bar{v}}{\partial y}. \quad (4)$$

In Eq. (4), the four terms on the right side represent the conversion of kinetic energy from MKE to EKE through the meridional shear of the zonal basic flow, the zonal shear of the meridional basic flow, the zonal convergence of the zonal basic flow, and the meridional

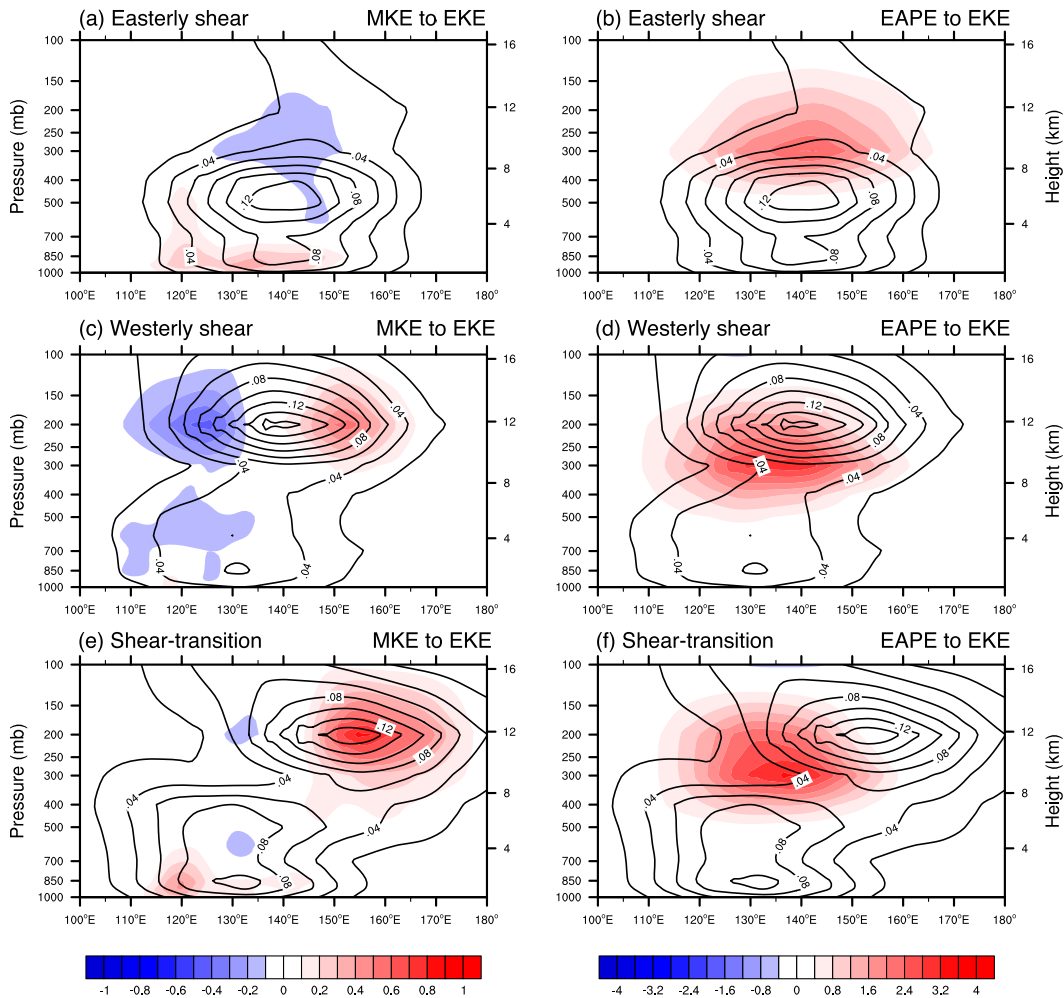


FIG. 9. EKE growth rate transitioning from time-mean kinetic energy (shaded; $10^{-6} \text{ m}^2 \text{ s}^{-3}$) in the (a) easterly sheared, (c) westerly sheared, and (e) shear transition categories, and the EKE growth rate transitioning from eddy available potential energy (shaded; $10^{-6} \text{ m}^2 \text{ s}^{-3}$) in the (b) easterly sheared, (d) westerly sheared, and (f) shear transition categories averaged between 10° and 20°N from lag day -5 to $+5$. Contours denote EKE ($\text{m}^2 \text{ s}^{-2}$).

convergence of the meridional basic flow. These terms are calculated at each pressure level by averaging values in the rectangular area of 10° – 20°N , 120° – 160°E . As shown in Table 2, the results suggest that the main source for EKE growth at 850 hPa in the easterly sheared environment is $-\overline{u'v'}\partial\overline{u}/\partial y$. In addition, the term $-\overline{u'^2}\partial\overline{u}/\partial x$ provides a second contribution. This term is

consistent with the common understanding that the cyclonic shear ($\partial\overline{u}/\partial y < 0$) and convergence ($\partial\overline{u}/\partial x < 0$) of zonal basic flow favor wave growth. However, as in the westerly sheared cases, the term $-\overline{v'^2}\partial\overline{v}/\partial y$ is responsible for the development of the upper-level wave, while the terms $-\overline{u'v'}\partial\overline{u}/\partial y$ and $-\overline{u'^2}\partial\overline{u}/\partial x$ are both negative. In shear transition basic flow, the upper-level meridional

TABLE 2. Each barotropic conversion term ($10^{-6} \text{ m}^2 \text{ s}^{-3}$) averaged over the western North Pacific (10° – 20°N , 120° – 160°E).

	Level (hPa)	$\partial\overline{K'}/\partial t$	$-\overline{u'v'}\partial\overline{u}/\partial y$	$-\overline{u'v'}\partial\overline{v}/\partial x$	$-\overline{u'^2}\partial\overline{u}/\partial x$	$-\overline{v'^2}\partial\overline{v}/\partial y$
Easterly shear	200	−0.78	−0.37	0.03	−0.28	−0.16
	850	1.91	1.91	−0.05	0.34	−0.28
Westerly shear	200	0.74	−1.82	0.03	−0.53	3.07
	850	0.06	0.40	0.04	0.14	−0.50
Shear transition	200	2.07	0.43	0.08	−0.71	2.28
	850	1.22	1.43	0.05	0.41	−0.67

convergence $-\overline{v^2} \partial \bar{v} / \partial y$ and the lower-level zonal wind shear $-\overline{u^2} \partial \bar{u} / \partial y$ induce the growth of transient eddies in the upper and lower troposphere, respectively.

Barotropic energy conversion is closely related to horizontal mean flow; thus, the different sheared circulation patterns and corresponding energy conversions are examined simultaneously, as shown in Fig. 10. The low-level pattern associated with the easterly sheared cases shows a typical circulation with a strong monsoon trough extending to approximately 150°E (Fig. 10a). Affected by the favorable meridional shear of the zonal mean flow, the positive EKE tendency appears as an elongated belt in the vicinity of the monsoon trough. Consequently, lower-tropospheric transient eddies quickly intensify over these regions. However, as shown in Fig. 10c, low-level circulation results in strong easterlies near the equator in the westerly sheared environment, which is similar to the circulation that occurs during transition periods between the East Asian summer and winter monsoons. The positive EKE tendency forms an east–west-oriented narrow belt to the south of 12°N, and the negative EKE tendency appears near the South China Sea. Because of the slower conversion rate of EKE, the lower-level disturbances grow slowly relative to those in the easterly sheared flow. Moreover, in the shear transition category, a monsoon trough is located over the western North Pacific (Fig. 10e) and consists of relatively weaker southwesterlies and stronger trade easterlies than in the easterly shear.

In the upper troposphere, all three cases show a high ridge with anticyclonic flow extending eastward from the East Asian continent, the tropical upper-tropospheric trough (TUTT), and divergent northeast flows near low-latitude areas (Figs. 10b,d,f). In the easterly shear, no upper-tropospheric growth occurs, even in the vicinity of the TUTT (Fig. 10b). This is attributed to the fact that easterly shear at lower latitudes traps Rossby waves in the lower-troposphere; thus, the upper-level counterparts are weaker and less organized. However, in westerly sheared cases, the high ridge is found farther south, with stronger westerlies to the north. The TUTT strengthens and extends westward to 150°E. Because of the southward shift of the TUTT, favorable meridional convergence of the basic flow can intrude farther west, which favors the growth of transient eddies (Fig. 10d) and further westward propagation of upper-level disturbances (Fig. 4b).

As suggested above, the shear transition cases consist of a combination of easterly and westerly sheared ambient flows, and the EKE growth caused by horizontal basic flow shows combination features as well. In the shear transition, the lower-level features are similar to those in the easterly shear cases, in that a strong monsoon trough exists and favors EKE growth in the lower

levels; and upper-level features are similar to those in westerly shear cases, in that a strong TUTT exists and favors EKE growth in the upper levels (Fig. 10f). These results are generally consistent with those of Wu et al. (2015b). Because the easterly shear traps waves in the lower troposphere and the westerly shear traps waves in the upper troposphere, the role of horizontal mean flow on synoptic-scale waves through barotropic conversions is in phase with the effect of vertical wind shear.

c. Change in eddy kinetic energy with westward propagation

The abovementioned results provide a general understanding of the EKE budget that affects TD-type waves in different sheared background flows. This section discusses the mechanisms for low-level growth when a TD-type disturbance penetrates an easterly sheared basic flow from a westerly sheared basic flow.

In Eq. (3), the third, fourth, and fifth terms represent the redistribution of EKE. The third term, $-V' \cdot \nabla \Phi' = -\overline{V'_h} \cdot \nabla_h \Phi' - \omega' \partial \Phi' / \partial z$, and the vertical component (the second term on the right side) are almost offset by the conversion from EAPE to EKE. The fourth term in Eq. (3) is the horizontal transport of EKE, and the fifth term is the direct vertical transport of EKE. When considering the EKE budget for a certain pressure level (e.g., 850 hPa), vertical transport is an additional source for EKE growth. Vertical transport is represented by the sum of the transport by basic flow and eddy fluctuation. In this calculation, basic flow transport dominates.

Regarding the shear transition cases, disturbances are identified by tracing the vortex center at each level regressed from lag day -5 to lag day $+5$. Daily EKE changes are acquired at 850, 500, and 200 hPa, respectively, by averaging the EKE in a $10^\circ \times 10^\circ$ rectangle around the vortex. As shown in Fig. 11a, the EKE at 200 hPa grows before lag day -3 and then rapidly decays. However, the EKEs at 500 and 850 hPa grow gradually before lag day $+1$ and lag day $+3$, respectively. The change in vertical wind shear is also plotted in Fig. 11a for reference.

The barotropic conversion and vertical transport terms in Eq. (3) are also calculated and shown in Figs. 11b–d for each level. In Fig. 11b, the barotropic energy conversion at 200 hPa is large before lag day -3 , which strengthens the upper-level disturbances. Then, after lag day -2 , this term becomes negative, which weakens the upper-level disturbances. Meanwhile, the vertical transport is much smaller, and the sign of the vertical transport is generally opposite the sign of the barotropic conversion term. After lag day 0, these two terms are small. Thus, the conversion from MKE to EKE controls the growth and decay of EKE in the

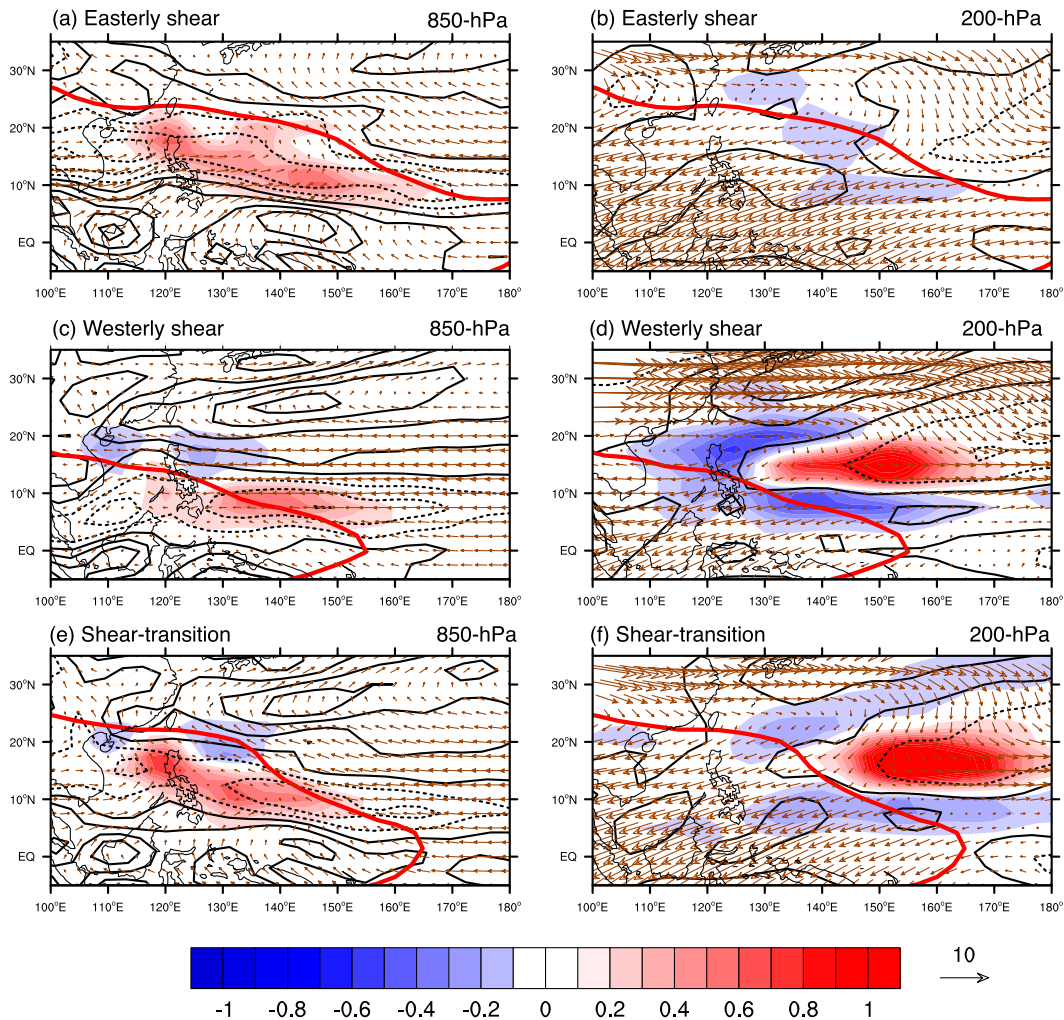


FIG. 10. Horizontal mean flow (vectors), EKE growth rate transitioning from the time-mean kinetic energy (shaded; $10^{-6} \text{ m}^2 \text{ s}^{-3}$) and $\partial \bar{u} / \partial y$ (black contours; 10^{-6} s^{-1}) at 850 hPa in the (a) easterly sheared, (c) westerly sheared, and (e) shear transition categories and at 200 hPa in the (b) easterly sheared, (d) westerly sheared, and (f) shear transition categories, except for $\partial \bar{u} / \partial y$ (black contour; 10^{-6} s^{-1}), averaged from lag day -5 to $+5$. The heavy red line denotes the zero value of vertical wind shear.

upper troposphere. At 500 hPa, as shown in Fig. 11c, the barotropic energy conversion term is positive before lag day 0. Then the vertical transport is approximately half of the barotropic conversion term, which implies that the conversion from MKE to EKE and the direct vertical transport are both important for midlevel development before penetrating the easterly sheared flow. The downward transport occurs before lag day 0, when the vertical wind shear changes from positive (westerly shear) to negative (easterly shear), as shown in Fig. 11c. The maximum downward transition is found at lag day -2 , when the magnitude of vertical shear is at a minimum. This implies that the downward transition is controlled by the change in vertical wind shear. At 850 hPa, the barotropic energy conversion is responsible

for EKE growth, and the contributions of vertical direct transport are negligible, as shown in Fig. 11d. The maximum growth rate according to barotropic energy conversion occurs at lag day $+1$ and is followed by a gradual decrease of the growth rate at 850 hPa.

The variation in the barotropic conversion is generally consistent with the change in the EKE at each pressure level. This demonstrates that the EKE growth/decay of a TD-type disturbance is mainly attributed to the energy conversion from the horizontal basic flow at each pressure level as the disturbance penetrates into the easterly sheared basic flow from the westerly sheared basic flow. The direct transport of EKE in the vertical direction mainly occurs at intermediate levels and is also important for midlevel EKE growth. As shown in Fig. 8, this

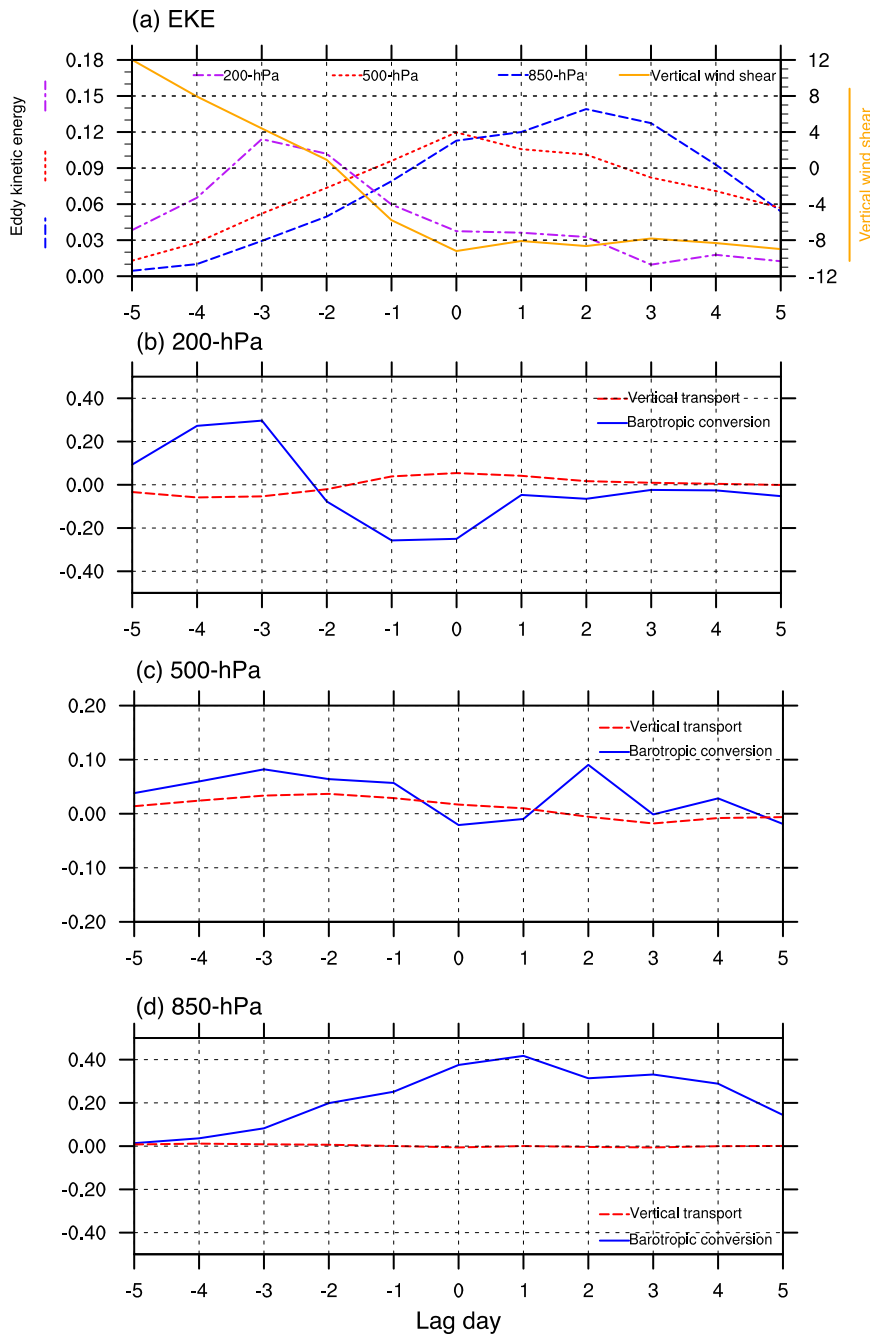


FIG. 11. (a) EKE ($\text{m}^2 \text{s}^{-2}$) variations at 850 (solid blue), 500 (dashed red), and 200 hPa (dashed purple) and vertical wind shear (solid orange; m s^{-1}) from lag day -5 to $+5$. Variations in the barotropic conversion term (solid blue; $10^{-6} \text{m}^2 \text{s}^{-3}$) and vertical transport term (dashed red; $10^{-6} \text{m}^2 \text{s}^{-3}$) from lag day -5 to $+5$ at (b) 200, (c) 500, and (d) 850 hPa. The results are averaged for the $10^\circ \times 10^\circ$ rectangle around the center of the vortex at each pressure level.

vertical direct transport can be dominated by direct downward transport. The results also suggest that the direct downward transition is controlled by the changes in the vertical wind shear. However, this direct downward

transport is negligible for upper- or lower-tropospheric wave growth. It should be noted that the upper-level disturbance becomes weaker following lag day -3 , which is different from the results shown in Fig. 8. This

difference occurs because the vortices are traced at upper and lower levels in this section, respectively, and are traced only at the lower level in Fig. 8.

5. Conclusions and discussion

This study presents a statistical analysis of the characteristics and energetics of TD-type waves under different vertically sheared background flows over the western North Pacific from June to November, 1979–2013, based on the reanalysis of NCEP–DOE AMIP-II and OLR data. The observations indicate that there are significant differences in the horizontal and vertical structures of synoptic-scale waves between different circulation patterns associated with vertical wind shear. In easterly sheared environments, the synoptic-scale waves propagate in the lower troposphere with a slightly westward tilt, and the vertical velocity has an eastward tilt with height. This structure suggests a positive feedback between the deep convection and low-level circulation in the “moisture mode” or “wave CISK” frameworks. This positive feedback induces enhanced boundary convergence and latent heat release by deep convection, thus leading to wave development in the lower troposphere. However, in westerly sheared environments, the wave propagates in the upper troposphere with a significant westward tilt, but the vertical motion is less vertically tilted. The wave-CISK mechanism is not the significant mechanism for these disturbances in the westerly sheared environment.

Next, an EKE budget diagnosis is conducted to investigate the physical mechanisms in the different cases. The results show that the conversion between MKE and EKE is responsible for the lower-level development in the easterly sheared environment and for the upper-level development in the westerly sheared environment. Further analyses indicate that the lower-level conversion occurs through the shear and the convergence of the zonal mean flow associated with the monsoon trough and that the upper-level conversion occurs through the convergence of the meridional mean flow associated with the TUTT. These consequences are consistent with the effect of vertical wind shear. When the disturbances are trapped in the lower level by easterly (westerly) shear, the horizontal mean flow also favors wave growth in the lower (upper) level. On the other hand, the transition from EAPE to EKE is several times larger than from MKE to EKE. This suggests that the conversion from EAPE to EKE is the major energy source driving these TD-type waves over the western North Pacific. But this conversion only occurs near the middle to upper troposphere, which is

less related to wave growth in either the upper troposphere or lower troposphere. In other words, the conversion from EAPE to EKE is less responsible for the wave growth and decay. Moreover, the conversion rate in the easterly sheared environment is smaller than that in the westerly sheared environment. This finding could be attributed to the weaker vertical motion and the phase difference between the temperature and vertical velocity anomalies resulting from the eastward tilt of vertical velocity in the easterly sheared background. This implies that the transition from EAPE to EKE is more important for the synoptic-scale waves in the westerly shear.

The current study also examines the evolution of a TD-type disturbance propagating from a westerly sheared environment to an easterly sheared environment. While the synoptic-scale disturbance crosses the critical longitude that divides the easterly shear from the westerly shear, the upper-level disturbance rapidly becomes weaker because of an unfavorable horizontal mean flow. Meanwhile, the lower-level disturbance quickly becomes stronger through the conversion from MKE to EKE. Observational and energetic analyses both indicate that the direct downward transport of the upper-tropospheric EKE occurs when the wave crosses the critical longitude. However, quantitative calculations suggest that downward transport is important only at intermediate levels and is negligible in the lower troposphere. Consequently, barotropic energy conversion is the most important kinetic energy source responsible for wave growth in the lower troposphere when the disturbance penetrates easterly sheared flows. The processes explaining this result are summarized as follows: When a synoptic-scale disturbance appears near the central Pacific, the westerly shear traps the disturbance in the upper troposphere, and the TUTT feeds MKE to the eddies, which favors upper-level growth. With westward propagation and penetration of the easterly sheared flow, the upper-level kinetic energy travels downward to the intermediate troposphere, which affects the midlevel wave growth. Meanwhile, the vertical structure of the lower-tropospheric disturbance is modified by easterly shear, and favorable zonal wind shear of the lower-tropospheric monsoon trough destabilizes the low-level disturbance by feeding MKE to EKE. Thus, the low-level TD-type disturbances strengthen through the barotropic energy conversion and the positive feedback between low-level circulation and deep convection.

This study suggests that vertical wind shear and low-level zonal wind shear are responsible for the lower-level growth of a westward-propagating wave when the upper-level disturbance penetrates the easterly sheared environment over the western North Pacific. The

quantitative calculations suggest that the downward transition does not intensify the low-level vortex directly. The role of the downward energy transition may be to induce an enclosed low-level vortex with enough intensification. Then further development of the vortex is attributed to the low-level horizontal mean flow and the convection–circulation feedback. Tam and Li (2006) also suggested that the downward wave activity is found near 400–700 hPa, which is consistent with the present results. Zhou and Wang (2007) also made a similar speculation when they studied a transition case from an upper-level MRG wave to a lower-level TD-type wave. Thus, the current study supports the findings by Tam and Li (2006) that low-level TD-type waves originate from upper-tropospheric disturbances over the western North Pacific.

However, some issues remain regarding the roles of vertically sheared ambient flow in westward-propagating waves. For example, the horizontal and vertical structures of a TD-type disturbance in the lower troposphere are similar to previous observational studies (e.g., Reed and Recker 1971; Lau and Lau 1990; Takayabu and Nitta 1993). However, the upper-tropospheric structure in the easterly shear is quite different. This requires further investigation. Additionally, the low-level EKE growth even appears inside the westerly sheared environment, despite the tendency of the westerly shear to trap waves in the upper troposphere, as shown in Fig. 10c. Although the vertical wind shear is substantially controlled by the horizontal flow between the upper and lower levels, low-level convergence can also be large when the sign of the vertical wind shear is positive. In this case, can the low-level disturbance develop and even become a tropical cyclone under westerly shear after several days? What is the role of coupled convection? Takayabu and Nitta (1993) suggested wave-CISK was not associated with TD-type waves because the tilting with height of vertical velocity was not observed. However, the current study reveals that the vertical velocity is clearly eastward tilted with height in easterly sheared environments and transitional environments, which supports the existence of a positive feedback between diabatic effects and circulation for these disturbances. Furthermore, Serra et al. (2008) suggested that TD-type waves feature downward energy dispersion while propagating westward near the central Pacific. However, the present study cannot find a significant signal associated with the vertical propagation of group velocity over the western North Pacific. More studies should be conducted on these issues to provide further understanding of the effects of vertically sheared background flow on tropical waves.

Acknowledgments. The authors are grateful to George N. Kiladis and two other anonymous reviewers for their insightful comments. We also thank Guanghua Chen for providing valuable discussion and suggestions. This work is jointly supported by the National Natural Science Foundation of China under Grants 41405067, 41330420, 41621005, 41461164005, and 41375065, and by the National Basic Research Program of China under Grant 2012CB417203.

REFERENCES

- Aiyyer, A. R., and J. Molinari, 2003: Evolution of mixed Rossby–gravity waves in idealized MJO environments. *J. Atmos. Sci.*, **60**, 2837–2855, doi:10.1175/1520-0469(2003)060<2837:EOMRWI>2.0.CO;2.
- Bolton, D., 1980: Application of the Miles theorem to forced linear perturbations. *J. Atmos. Sci.*, **37**, 1639–1642, doi:10.1175/1520-0469(1980)037<1639:AOTMTT>2.0.CO;2.
- Boyd, J. P., 1978a: The effects of latitudinal shear on equatorial waves. Part I: Theory and methods. *J. Atmos. Sci.*, **35**, 2236–2258, doi:10.1175/1520-0469(1978)035<2236:TEOLSO>2.0.CO;2.
- , 1978b: The effects of latitudinal shear on equatorial waves. Part II: Applications to the atmosphere. *J. Atmos. Sci.*, **35**, 2259–2267, doi:10.1175/1520-0469(1978)035<2259:TEOLSO>2.0.CO;2.
- Chang, C. P., V. F. Morris, and J. M. Wallace, 1970: A statistical study of easterly waves in the western Pacific: July–December 1964. *J. Atmos. Sci.*, **27**, 195–201, doi:10.1175/1520-0469(1970)027<0195:ASSOEW>2.0.CO;2.
- Chen, G., 2012: A comparison of the transition of equatorial waves between two types of ENSO events in a multilevel model. *J. Atmos. Sci.*, **69**, 2364–2378, doi:10.1175/JAS-D-11-0292.1.
- , and R. Huang, 2009: Interannual variations in mixed Rossby–gravity waves and their impacts on tropical cyclogenesis over the western North Pacific. *J. Climate*, **22**, 535–549, doi:10.1175/2008JCLI2221.1.
- , and C.-H. Sui, 2010: Characteristics and origin of quasi-biweekly oscillation over the western North Pacific during boreal summer. *J. Geophys. Res.*, **115**, D14113, doi:10.1029/2009JD013389.
- , and C.-Y. Tam, 2012: A new perspective on the excitation of low-tropospheric mixed Rossby–gravity waves in association with energy dispersion. *J. Atmos. Sci.*, **69**, 1397–1403, doi:10.1175/JAS-D-11-0331.1.
- , and C. Chou, 2014: Joint contribution of multiple equatorial waves to tropical cyclogenesis over the western North Pacific. *Mon. Wea. Rev.*, **142**, 79–93, doi:10.1175/MWR-D-13-00207.1.
- Davies, H. C., 1979: Phase-lagged wave-CISK. *Quart. J. Roy. Meteor. Soc.*, **105**, 325–353, doi:10.1002/qj.49710544402.
- Dickinson, M., and J. Molinari, 2002: Mixed Rossby–gravity waves and western Pacific tropical cyclogenesis. Part I: Synoptic evolution. *J. Atmos. Sci.*, **59**, 2183–2196, doi:10.1175/1520-0469(2002)059<2183:MRGWAW>2.0.CO;2.
- Dunkerton, T. J., and M. P. Baldwin, 1995: Observation of 3–6-day meridional wind oscillations over the tropical Pacific, 1973–1992: Horizontal structure and propagation. *J. Atmos. Sci.*, **52**, 1585–1601, doi:10.1175/1520-0469(1995)052<1585:OODMWO>2.0.CO;2.
- Feng, T., G. H. Chen, R. H. Huang, and X. Y. Shen, 2014: Large-scale circulation patterns favourable to tropical cyclogenesis

- over the western North Pacific and associated barotropic energy conversions. *Int. J. Climatol.*, **34**, 216–227, doi:10.1002/joc.3680.
- Frank, W. M., and P. E. Roundy, 2006: The role of tropical waves in tropical cyclogenesis. *Mon. Wea. Rev.*, **134**, 2397–2417, doi:10.1175/MWR3204.1.
- Fu, B., T. Li, M. S. Peng, and F. Weng, 2007: Analysis of tropical cyclogenesis in the western North Pacific for 2000 and 2001. *Wea. Forecasting*, **22**, 763–780, doi:10.1175/WAF1013.1.
- Ge, X., T. Li, and X. Zhou, 2007: Tropical cyclone energy dispersion under vertical shears. *Geophys. Res. Lett.*, **34**, L23807, doi:10.1029/2007GL031867.
- , —, Y. Wang, and M. S. Peng, 2008: Tropical cyclone energy dispersion in a three-dimensional primitive equation model: Upper-tropospheric influence. *J. Atmos. Sci.*, **65**, 2272–2289, doi:10.1175/2007JAS2431.1.
- Han, Y., and B. Khouider, 2010: Convectively coupled waves in a sheared environment. *J. Atmos. Sci.*, **67**, 2913–2942, doi:10.1175/2010JAS3335.1.
- Hayashi, Y., 1970: A theory of large-scale equatorial waves generated by condensation heat and accelerating. *J. Meteor. Soc. Japan*, **48**, 140–160.
- Holland, G. J., 1995: Scale interaction in the western Pacific monsoon. *Meteor. Atmos. Phys.*, **56**, 57–79, doi:10.1007/BF01022521.
- Holton, J. R., 1971: A diagnostic model for equatorial wave disturbances: The role of vertical shear of the mean zonal wind. *J. Atmos. Sci.*, **28**, 55–64, doi:10.1175/1520-0469(1971)028<0055:ADMFEW>2.0.CO;2.
- , 2004: *An Introduction to Dynamic Meteorology*. 4th ed. Elsevier Academic Press, 535 pp.
- Huang, P., and R. Huang, 2011: Climatology and interannual variability of convectively coupled equatorial waves activity. *J. Climate*, **24**, 4451–4465, doi:10.1175/2011JCLI4021.1.
- Kanamitsu, M., W. Ebisuzaki, J. Woollen, S.-K. Yang, J. J. Hnilo, M. Fiorino, and G. L. Potter, 2002: NCEP–DOE AMIP-II reanalysis (R-2). *Bull. Amer. Meteor. Soc.*, **83**, 1631–1643, doi:10.1175/BAMS-83-11-1631.
- Kiladis, G. N., J. Dias, and M. Gehne, 2016: The relationship between equatorial mixed Rossby–gravity and eastward inertio-gravity waves. Part I. *J. Atmos. Sci.*, **73**, 2123–2145, doi:10.1175/JAS-D-15-0230.1.
- Krouse, K. D., A. H. Sobel, and L. M. Polvani, 2008: On the wavelength of the Rossby waves radiated by tropical cyclones. *J. Atmos. Sci.*, **65**, 644–654, doi:10.1175/2007JAS2402.1.
- Kuo, H.-C., J.-H. Chen, R. T. Williams, and C. P. Chang, 2001: Rossby waves in zonally opposing mean flow: Behavior in Northwest Pacific summer monsoon. *J. Atmos. Sci.*, **58**, 1035–1050, doi:10.1175/1520-0469(2001)058<1035:RWIZOM>2.0.CO;2.
- Lane, T. P., M. J. Reeder, and T. L. Clark, 2001: Numerical modeling of gravity wave generation by deep tropical convection. *J. Atmos. Sci.*, **58**, 1249–1274, doi:10.1175/1520-0469(2001)058<1249:NMOGWG>2.0.CO;2.
- Lau, K.-H., and N.-C. Lau, 1990: Observed structure and propagation characteristics of tropical summertime synoptic scale disturbances. *Mon. Wea. Rev.*, **118**, 1888–1913, doi:10.1175/1520-0493(1990)118,1888:OSAPCO.2.0.CO;2.
- , and —, 1992: The energetics and propagation dynamics of tropical summertime synoptic-scale disturbances. *Mon. Wea. Rev.*, **120**, 2523–2539, doi:10.1175/1520-0493(1992)120,2523:TEAPDO.2.0.CO;2.
- Li, T., 2006: Origin of the summertime synoptic-scale wave train in the western North Pacific. *J. Atmos. Sci.*, **63**, 1093–1102, doi:10.1175/JAS3676.1.
- Liebmann, B., and H. H. Hendon, 1990: Synoptic-scale disturbances near the equator. *J. Atmos. Sci.*, **47**, 1463–1479, doi:10.1175/1520-0469(1990)047<1463:SSDNTE>2.0.CO;2.
- , and C. A. Smith, 1996: Description of a complete (interpolated) outgoing longwave radiation dataset. *Bull. Amer. Meteor. Soc.*, **77**, 1275–1277.
- Lindzen, R. S., 1974: Wave-CISK in the tropics. *J. Atmos. Sci.*, **31**, 156–179, doi:10.1175/1520-0469(1974)031<0156:WCITT>2.0.CO;2.
- Lipps, F. B., 1970: Barotropic stability and tropical disturbances. *Mon. Wea. Rev.*, **98**, 122–131, doi:10.1175/1520-0493(1970)098<0122:BSATD>2.3.CO;2.
- Livezey, R. E., and W. Y. Chen, 1983: Statistical field significance and its determination by Monte Carlo techniques. *Mon. Wea. Rev.*, **111**, 46–59, doi:10.1175/1520-0493(1983)111<0046:SFSAID>2.0.CO;2.
- Maloney, E. D., and D. L. Hartmann, 2001: The Madden–Julian oscillation, barotropic dynamics, and North Pacific tropical cyclone formation. Part I: Observations. *J. Atmos. Sci.*, **58**, 2545–2558, doi:10.1175/1520-0469(2001)058<2545:TMJOBDD>2.0.CO;2.
- Mapes, B. E., 2000: Convective inhibition, subgrid-scale triggering energy, and stratiform instability in a toy tropical wave model. *J. Atmos. Sci.*, **57**, 1515–1535, doi:10.1175/1520-0469(2000)057<1515:CISSTE>2.0.CO;2.
- Molinari, J., K. Lombardo, and D. Vollaro, 2007: Tropical cyclogenesis within an equatorial Rossby wave packet. *J. Atmos. Sci.*, **64**, 1301–1317, doi:10.1175/JAS3902.1.
- NCEP/NWS/NOAA/DOC, 2000: NCEP/DOE Reanalysis 2 (R2). Research Data Archive at the National Center for Atmospheric Research, Computational and Information Systems Laboratory, accessed 11 August 2015. [Available online at <http://rda.ucar.edu/datasets/ds091.0/>.]
- Nitta, T., and M. Yanai, 1969: A note on the barotropic instability of the tropical easterly current. *J. Meteor. Soc. Japan*, **47**, 127–130.
- , and Y. Takayabu, 1985: Global analysis of the lower tropospheric disturbances in the tropics during the northern summer of the FGGE year part II: Regional characteristics of the disturbances. *Pure Appl. Geophys. (PAGEOPH)*, **123**, 272–292, doi:10.1007/BF00877023.
- NOAA/OAR/ESRL/PSD, 1996: NOAA interpolated outgoing longwave radiation (OLR). NOAA/ESRL/Physical Sciences Division, Data Management, accessed 5 February 2015. [Available online at http://www.esrl.noaa.gov/psd/data/gridded/data.interp_OLR.html.]
- Park, M. S., H. S. Kim, C. H. Ho, R. L. Elsberry, and M. I. Lee, 2015: Tropical Cyclone Mekkhala’s (2008) formation over the South China Sea: Mesoscale, synoptic-scale, and large-scale contributions. *Mon. Wea. Rev.*, **143**, 88–110, doi:10.1175/MWR-D-14-00119.1.
- Raymond, D. J., and Ž. Fuchs, 2007: Convectively coupled gravity and moisture modes in a simple atmospheric model. *Tellus*, **59A**, 627–640, doi:10.1111/j.1600-0870.2007.00268.x.
- Reed, R. J., and E. E. Recker, 1971: Structure and properties of synoptic-scale wave disturbances in the equatorial western Pacific. *J. Atmos. Sci.*, **28**, 1117–1133, doi:10.1175/1520-0469(1971)028<1117:SAPOSS>2.0.CO;2.
- Schreck, C. J., J. Molinari, and K. I. Mohr, 2011: Attributing tropical cyclogenesis to equatorial waves in the western North Pacific. *J. Atmos. Sci.*, **68**, 195–209, doi:10.1175/2010JAS3396.1.
- , —, and A. Aiyer, 2012: A global view of equatorial waves and tropical cyclogenesis. *Mon. Wea. Rev.*, **140**, 774–788, doi:10.1175/MWR-D-11-00110.1.

- Serra, Y. L., G. N. Kiladis, and M. F. Cronin, 2008: Horizontal and vertical structure of easterly waves in the Pacific ITCZ. *J. Atmos. Sci.*, **65**, 1266–1284, doi:[10.1175/2007JAS2341.1](https://doi.org/10.1175/2007JAS2341.1).
- Sobel, A. H., and C. S. Bretherton, 1999: Development of synoptic-scale disturbances over the summertime tropical northwest Pacific. *J. Atmos. Sci.*, **56**, 3106–3127, doi:[10.1175/1520-0469\(1999\)056<3106:DOSSDO>2.0.CO;2](https://doi.org/10.1175/1520-0469(1999)056<3106:DOSSDO>2.0.CO;2).
- , J. Nilsson, and L. M. Polvani, 2001: The weak temperature gradient approximation and balanced tropical moisture waves. *J. Atmos. Sci.*, **58**, 3650–3665, doi:[10.1175/1520-0469\(2001\)058<3650:TWTGAA>2.0.CO;2](https://doi.org/10.1175/1520-0469(2001)058<3650:TWTGAA>2.0.CO;2).
- Tai, K.-S., and Y. Ogura, 1987: An observational study of easterly waves over the eastern Pacific in the northern summer using FGGE data. *J. Atmos. Sci.*, **44**, 339–361, doi:[10.1175/1520-0469\(1987\)044<0339:AOSOEW>2.0.CO;2](https://doi.org/10.1175/1520-0469(1987)044<0339:AOSOEW>2.0.CO;2).
- Takayabu, Y. N., and T. Nitta, 1993: 3–5 day-period disturbances coupled with convection over the tropical Pacific Ocean. *J. Meteor. Soc. Japan*, **71**, 221–246.
- Tam, C. Y., and T. Li, 2006: The origin and dispersion characteristics of the observed tropical summertime synoptic-scale waves over the western Pacific. *Mon. Wea. Rev.*, **134**, 1630–1646, doi:[10.1175/MWR3147.1](https://doi.org/10.1175/MWR3147.1).
- Wallace, J. M., 1971: Spectral studies of tropospheric wave disturbances in the tropical western Pacific. *Rev. Geophys.*, **9**, 557–612, doi:[10.1029/RG009i003p00557](https://doi.org/10.1029/RG009i003p00557).
- Wang, B., and X. Xie, 1996: Low-frequency equatorial waves in vertically sheared zonal flow. Part I: Stable waves. *J. Atmos. Sci.*, **53**, 449–467, doi:[10.1175/1520-0469\(1996\)053<0449:LFEWIV>2.0.CO;2](https://doi.org/10.1175/1520-0469(1996)053<0449:LFEWIV>2.0.CO;2).
- Webster, P. J., and H.-R. Chang, 1988: Equatorial energy accumulation and emanation regions: Impacts of a zonally varying basic state. *J. Atmos. Sci.*, **45**, 803–829, doi:[10.1175/1520-0469\(1988\)045<0803:EEAER>2.0.CO;2](https://doi.org/10.1175/1520-0469(1988)045<0803:EEAER>2.0.CO;2).
- , and —, 1998: Atmospheric wave propagation in heterogeneous flow: Basic flow controls on tropical–extratropical interaction and equatorial wave modification. *Dyn. Atmos. Oceans*, **27**, 91–134, doi:[10.1016/S0377-0265\(97\)00003-1](https://doi.org/10.1016/S0377-0265(97)00003-1).
- Wheeler, M., and G. N. Kiladis, 1999: Convectively coupled equatorial waves: Analysis of clouds and temperature in the wavenumber–frequency domain. *J. Atmos. Sci.*, **56**, 374–399, doi:[10.1175/1520-0469\(1999\)056<0374:CCEWAO>2.0.CO;2](https://doi.org/10.1175/1520-0469(1999)056<0374:CCEWAO>2.0.CO;2).
- Wu, L., Z. Wen, R. Huang, and R. Wu, 2012: Possible linkage between the monsoon trough variability and the tropical cyclone activity over the western North Pacific. *Mon. Wea. Rev.*, **140**, 140–150, doi:[10.1175/MWR-D-11-00078.1](https://doi.org/10.1175/MWR-D-11-00078.1).
- , —, T. Li, and R. Huang, 2014: ENSO-phase dependent TD and MRG wave activity in the western North Pacific. *Climate Dyn.*, **42**, 1217–1227, doi:[10.1007/s00382-013-1754-4](https://doi.org/10.1007/s00382-013-1754-4).
- , —, and R. Wu, 2015a: Influence of the monsoon trough on westward-propagating tropical waves over the western North Pacific. Part I: Observations. *J. Climate*, **28**, 7108–7127, doi:[10.1175/JCLI-D-14-00806.1](https://doi.org/10.1175/JCLI-D-14-00806.1).
- , —, and —, 2015b: Influence of the monsoon trough on westward-propagating tropical waves over the western North Pacific. Part II: Energetics and numerical experiments. *J. Climate*, **28**, 9332–9349, doi:[10.1175/JCLI-D-14-00807.1](https://doi.org/10.1175/JCLI-D-14-00807.1).
- Xie, X., and B. Wang, 1996: Low-frequency equatorial waves in vertically sheared zonal flow. Part II: Unstable waves. *J. Atmos. Sci.*, **53**, 3589–3605, doi:[10.1175/1520-0469\(1996\)053,3589:LFEWIV.2.0.CO;2](https://doi.org/10.1175/1520-0469(1996)053,3589:LFEWIV.2.0.CO;2).
- Xu, Y., T. Li, and M. Peng, 2013: Tropical cyclogenesis in the western North Pacific as revealed by the 2008–09 YOTC data. *Wea. Forecasting*, **28**, 1038–1056, doi:[10.1175/WAF-D-12-00104.1](https://doi.org/10.1175/WAF-D-12-00104.1).
- , —, and —, 2014: Roles of the synoptic-scale wave train, the intraseasonal oscillation, and high-frequency eddies in the genesis of Typhoon Manyi (2001). *J. Atmos. Sci.*, **71**, 3706–3722, doi:[10.1175/JAS-D-13-0406.1](https://doi.org/10.1175/JAS-D-13-0406.1).
- Yang, G.-Y., B. Hoskins, and J. Slingo, 2003: Convectively coupled equatorial waves: A new methodology for identifying wave structures in observational data. *J. Atmos. Sci.*, **60**, 1637–1654, doi:[10.1175/1520-0469\(2003\)060<1637:CCEWAN>2.0.CO;2](https://doi.org/10.1175/1520-0469(2003)060<1637:CCEWAN>2.0.CO;2).
- Zhang, M., and M. A. Geller, 1994: Selective excitation of tropical atmospheric waves in wave-CISK: The effect of vertical wind shear. *J. Atmos. Sci.*, **51**, 353–368, doi:[10.1175/1520-0469\(1994\)051<0353:SEOTAW>2.0.CO;2](https://doi.org/10.1175/1520-0469(1994)051<0353:SEOTAW>2.0.CO;2).
- Zhou, X., and B. Wang, 2007: Transition from an eastern Pacific upper-level mixed Rossby–gravity wave to a western Pacific tropical cyclone. *Geophys. Res. Lett.*, **34**, L24801, doi:[10.1029/2007GL031831](https://doi.org/10.1029/2007GL031831).